

How Attention Sinks Emerge in Large Language Models: An Interpretability Perspective

Runyu Peng¹ Ruixiao Li² Mingshu Chen² Yunhua Zhou^{1†} Qipeng Guo^{1†} Xipeng Qiu^{2†}

¹Shanghai AI Laboratory, China

²Fudan University, China

{pengrunyu, zhoyunhua}@pjlab.org.cn

Large Language Models (LLMs) often allocate disproportionate attention to specific tokens, a phenomenon commonly referred to as the **attention sink**. While such sinks are generally considered detrimental, prior studies have identified a notable exception: the model’s consistent emphasis on the first token of the input sequence. This structural bias can influence a wide range of downstream applications and warrants careful consideration. Despite its prevalence, the precise mechanisms underlying the emergence and persistence of attention sinks remain poorly understood.

In this work, we trace the formation of attention sinks around the first token of the input. We identify a simple mechanism, referred to as the **P0-Sink Circuit**, that enables the model to recognize token at position zero and induce an attention sink within two transformer blocks, without relying on any semantic information. This mechanism serves as the basis for the attention sink on position zero. Furthermore, by analyzing training traces from a 30B-A3B MoE model trained from scratch, we find that this mechanism emerges early in training and becomes increasingly concentrated in the first two layers, suggesting a possible signal for tracking pre-training convergence states.

1. Introduction

Auto-regressive language models tend to allocate disproportionately large attention to initial tokens. This phenomenon, the **attention sink**, reflects how softmax attention assigns probability [16]. Sinks also appear at non-initial positions, where excessive and persistent focus on certain tokens can interfere with effective reasoning and reduce model accuracy [18]. Suppressing these sinks often leads to improved performance.

The main exception is the model’s consistent emphasis on the *first* token of the input. This **position-zero (P0) sink** is correlated with improved predictions and is used in several downstream applications [5, 10, 16]. Understanding why this effect emerges and how it is implemented within the model’s internal computation is a central objective of this study.

To this end, we conduct a deep investigation of the P0 sink. Firstly, we perform an ablation study on the Beginning-Of-Sequence ([BOS]) token. The results show that removing [BOS] only affects the first-layer attention pattern in modern LLMs [7], suggesting that the P0 sink is not merely a byproduct of [BOS] semantics, but rather a more fundamental mechanism. To reveal this mechanism, we propose the **P0-Sink Circuit**, a simple yet effective architectural component that exploits the asymmetry of the causal attention mask. This circuit enables the model to reliably detect position zero and transform it into a deterministic representation with amplified ℓ_2 norm. Such a high-norm, fixed-direction hidden state directly triggers the P0 sink effect, aligning with observations from previous studies [4, 8].

To empirically validate the formation of this mechanism, we pre-train a 30B-A3B MoE model from scratch and track the evolution of its attention patterns. We find that P0 sink first emerges in deep layers, temporarily diffuses across early positions in shallow layers, and converges with a P0-Sink Circuit within the first two layers.

† Corresponding author.

* Code is at <https://github.com/Account4PaperReview/SinkCircuit>

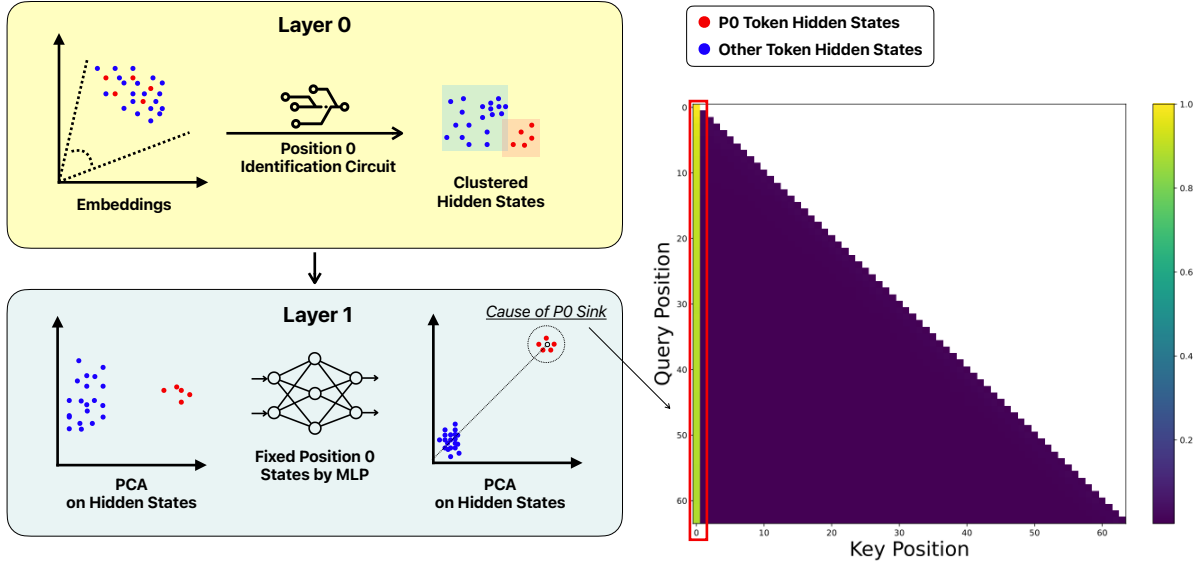


Figure 1: Overview of the proposed **P0-Sink Circuit**. Within just two transformer blocks, the model learns to identify the position-zero (P0) token and amplify it into a fixed high-norm representation, which gives rise to the attention sink effect.

In this work, we make the following contributions¹:

1. We demonstrate that the position-zero sink (**P0 sink**) arises from causal-masking asymmetry rather than [BOS] semantics.
2. We formalize the **P0-Sink Circuit**, a two-layer mechanism that exploits this asymmetry to generate a fixed and high-norm representation at position zero, which provides a consistent reference point for attention heads throughout the network.
3. We characterize the formation of P0-Sink Circuit as a three-stage process during pre-training: emerging in deeper layers, spreading among early positions in shallow layers, and concentrating in the first two layers.

¹All experiments are conducted on a subset of FineWeb-Edu dataset [11]

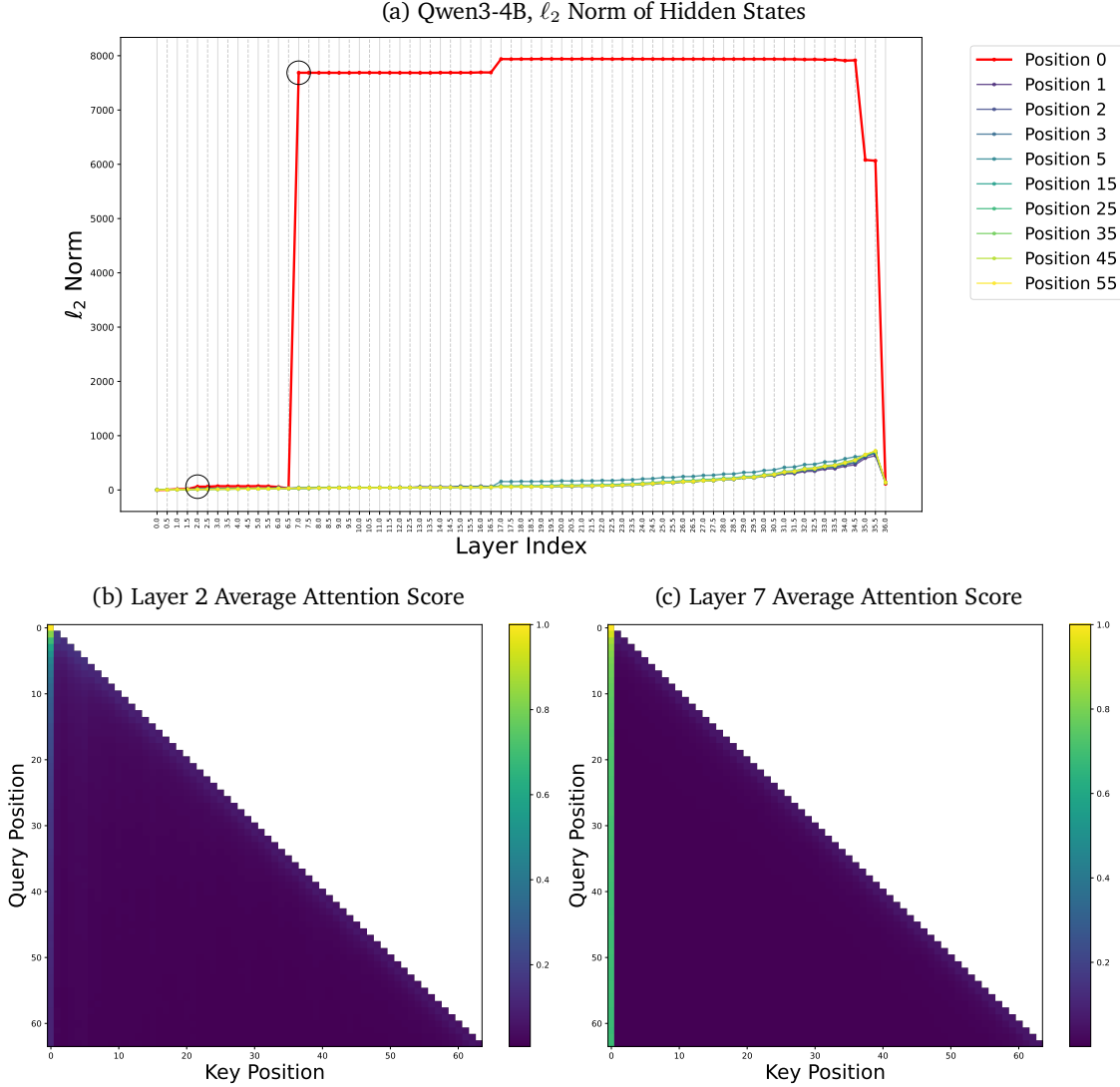


Figure 2: Layer-wise ℓ_2 norm of hidden states and attention score heat maps in Qwen3-4B. Although this model has no [BOS] token, its position-zero (P0) sink appears after layer 2 and becomes pronounced after layer 7, alongside an increase in the ℓ_2 norm at position zero. Half-integer layer indices denote attention outputs after the residual connection.

2. Related Works

P0 sink has long been the subject of investigation. Cancedda [4] associate it with significantly amplified ℓ_2 norms in the hidden states of the [BOS] token. They also observe linearity in these hidden states, which makes them suitable for analysis in specific linear subspaces. Barbero et al. [2] remove [BOS] and report a weakened sink effect, with the Sink Rate metric proposed by Gu et al. [8]. However, it turns out that this conclusion no longer holds for more recent LLMs, where the P0 sink is driven by structural mechanisms rather than the [BOS] embedding.

Zhang et al. [20] summarized several functional interpretations of attention sinks. For example, Gu et al. [8] argued that attention sinks introduce a soft inductive bias into the attention mechanism, compensating for the absence of explicit bias parameters in attention layers. Other studies propose that the P0 sink helps deactivate redundant attention heads [9, 15]. Additionally, P0 sink has been linked to stabilizing sequence structure, reducing over-mixing of token representations, and preventing rank collapse [2, 6]. While these work has proposed hypotheses highlighting the functional importance of the P0 sink, the concrete mechanisms by which large language models implement this behavior remain unclear.

First Token Repeat Time (n)		n=1	n=2	n=3	n=4	n=5	n=6	n=7	n=8
Llama-3.2-1B	w/ [BOS]	3.22	3.27	3.36	3.46	3.56	3.68	3.80	3.92
	w/o [BOS]	3.32	3.36	3.42	3.48	3.53	3.58	3.62	3.66
Llama-3.2-3B	w/ [BOS]	2.97	3.01	3.07	3.15	3.23	3.33	3.43	3.53
	w/o [BOS]	3.06	3.10	3.15	3.19	3.22	3.26	3.29	3.32
Llama-3.1-8B	w/ [BOS]	2.66	2.68	2.72	2.76	2.80	2.84	2.89	2.93
	w/o [BOS]	2.79	2.81	2.83	2.85	2.86	2.88	2.89	2.90
Mistral-7B-v0.3	w/ [BOS]	2.44	2.46	2.49	2.54	2.60	2.69	2.79	2.91
	w/o [BOS]	2.39	2.39	2.40	2.41	2.41	2.42	2.43	2.44

Table 1: Loss variation under different first-token repeat counts. **Bold** indicates the smaller loss between the two settings at each repeat count. In the w/ [BOS] setting, the repeated token is [BOS]; in the w/o [BOS] setting, the first content token is repeated after removing [BOS]. For both settings, losses on repeated tokens and the original [BOS] position are excluded from evaluation, ensuring a consistent number of evaluated tokens across conditions for fair comparison.

3. Is [BOS] Token Necessary for P0 Sink?

Cancedda [4] identify a key internal mechanism underlying the attention sink phenomenon: the hidden states of a fixed [BOS] token exhibit significantly amplified ℓ_2 norms after passing through certain transformer layers. Building on this, Gu et al. [8] further investigate the correlation between this norm inflation and the emergence of attention sinks, showing that attention scores become disproportionately concentrated on the P0 tokens as a result.

Subsequent works have shown that the attention sink phenomenon also arises in models without an explicit [BOS] token [15]. For example, in the Qwen and OLMo model families [12, 14, 17], the P0 token, typically corresponding to the first non-padding token, continues to attract a dominant share of attention across layers and heads. Notably, this behavior is again accompanied by a significant increase in the ℓ_2 norm of the P0 token’s hidden states as it propagates through the network, shown in Figure 2.

In models such as LLaMA [7], removing the [BOS] token leads to a measurable increase in training loss and degrades downstream performance [2], suggesting that [BOS] plays a nontrivial functional role. However, as shown in Figure 3, a clear attention sink at position zero re-emerges after several layers even in the absence of [BOS], indicating that this behavior cannot be fully explained by the [BOS] embedding itself. The model learns a second mechanism, operating through deeper MLP sublayers, that stabilizes the P0 representation independently of [BOS].

This division of labor becomes more evident when comparing shallow versus deep layers. While [BOS] influences early hidden states, deeper layers consistently reconstruct a fixed direction for position zero through specific MLP sublayers, regardless of the initial token. Table 1 further supports this view by showing that such deeper mechanisms remain robust across input perturbations.

One such perturbation arises from a known property of modern positional encoding schemes. Since position is encoded via relative or rotary mechanisms, repeating the first token causes multiple positions to share nearly identical hidden states [8], creating a synthetic prefix pattern that deviates from the model’s training distribution—a form of out-of-distribution (OOD) shift.

The position-zero sink re-emerges under such diverse conditions highlights the stability of this [BOS]-independent mechanism. This motivates a detailed examination of its formation, as it may offer a more general and robust inductive bias than token-based schemes, and may help LLMs maintain coherence under OOD inputs such as long contexts.

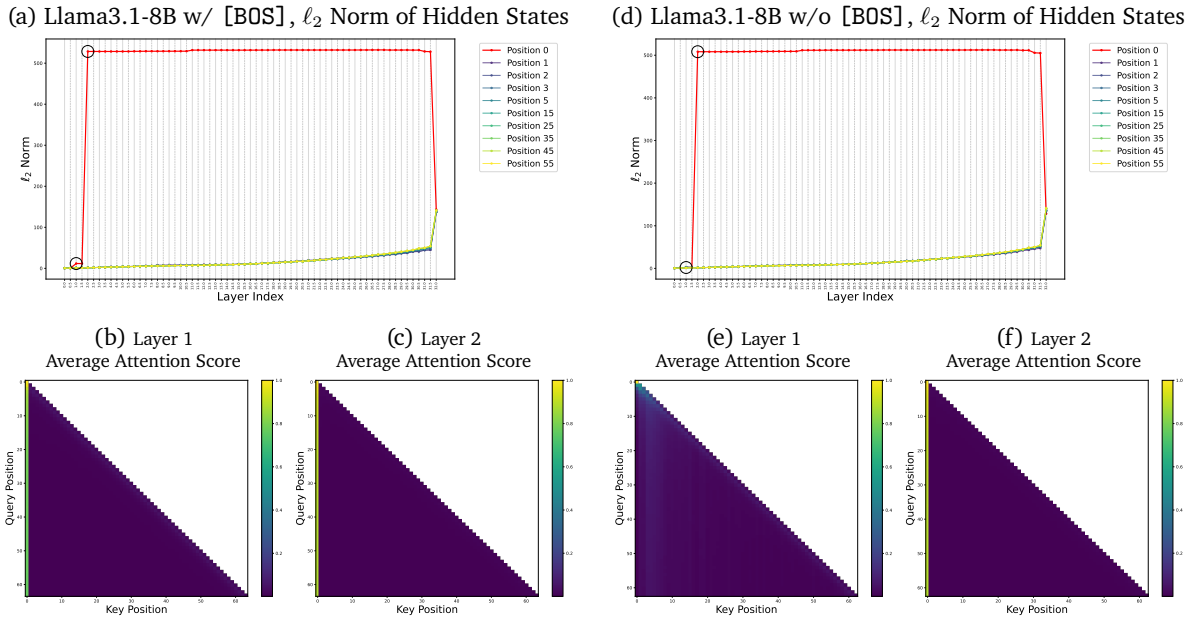


Figure 3: Layer-wise ℓ_2 norm of hidden states and attention score heat maps in LLaMA3.1-8B. Half-integer indices correspond to the output of attention modules after residual connection. Removing the [BOS] token eliminates the layer-1 attention sink and its associated ℓ_2 norm amplification. However, due to renewed norm growth before layer 2, a position-zero (P0) sink re-emerges in the attention maps even in the absence of the [BOS] token.

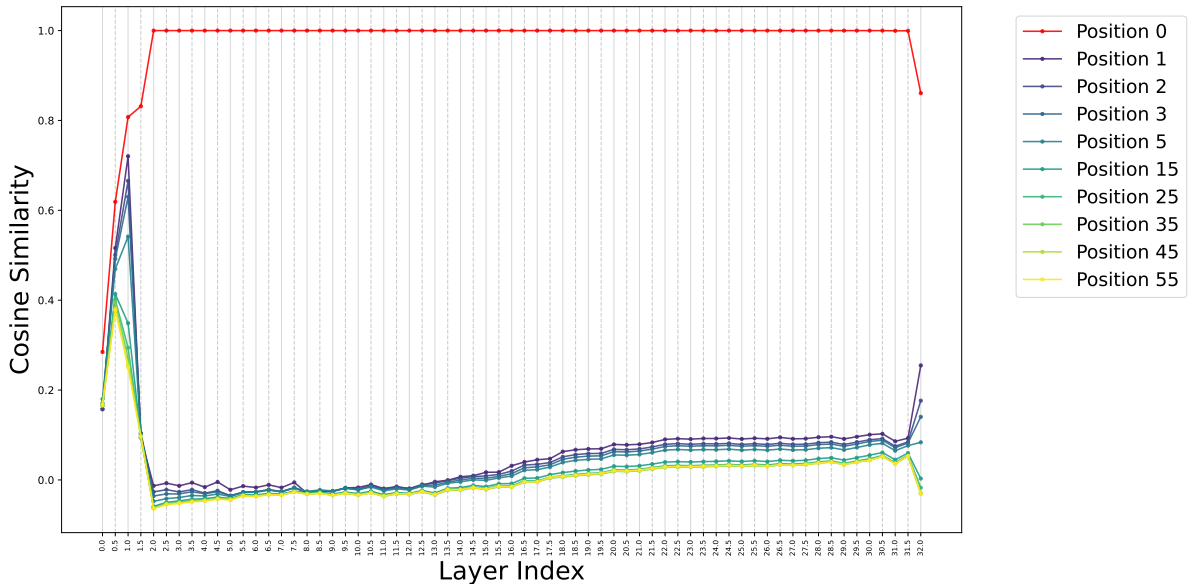


Figure 4: Average cosine similarity among hidden states at different positions across inputs, along with the corresponding mean hidden state vectors at position zero in LLaMA3.1-8B. Half-integer indices indicate the outputs of attention modules after residual addition. The [BOS] token has been removed, so position zero corresponds to the first non-[BOS] token.

4. How LLMs Sink the Position-Zero Token

4.1. Fixed Representation at Position Zero

Figure 3 demonstrates that even after removing the [BOS] token from a model trained with it, the model still successfully localizes the position-zero (P0) token within just two transformer blocks. Notably, the MLP further amplifies the hidden state at this position by increasing its ℓ_2 norm. Figure 4 reveals that the MLP not only increases the magnitude, but also projects the P0 hidden state toward a consistent direction in the representation space.

This amplification brings two key benefits. First, it reduces the influence of token embeddings on the representation of position zero. Since the MLP output is added to the residual stream, the amplified hidden state at P0 dominates the combined representation, effectively suppressing earlier-layer contributions that are several orders of magnitude smaller.

Second, when combined with the pre-layer RMS normalization (pre-norm) commonly used in modern LLMs [1, 19], the amplified norm helps stabilize the P0 representation during training. A high-magnitude vector is less sensitive to gradient updates and more likely to preserve its direction across optimization steps. This stability enables the model to maintain a consistent and distinguishable representation of P0 tokens throughout training.

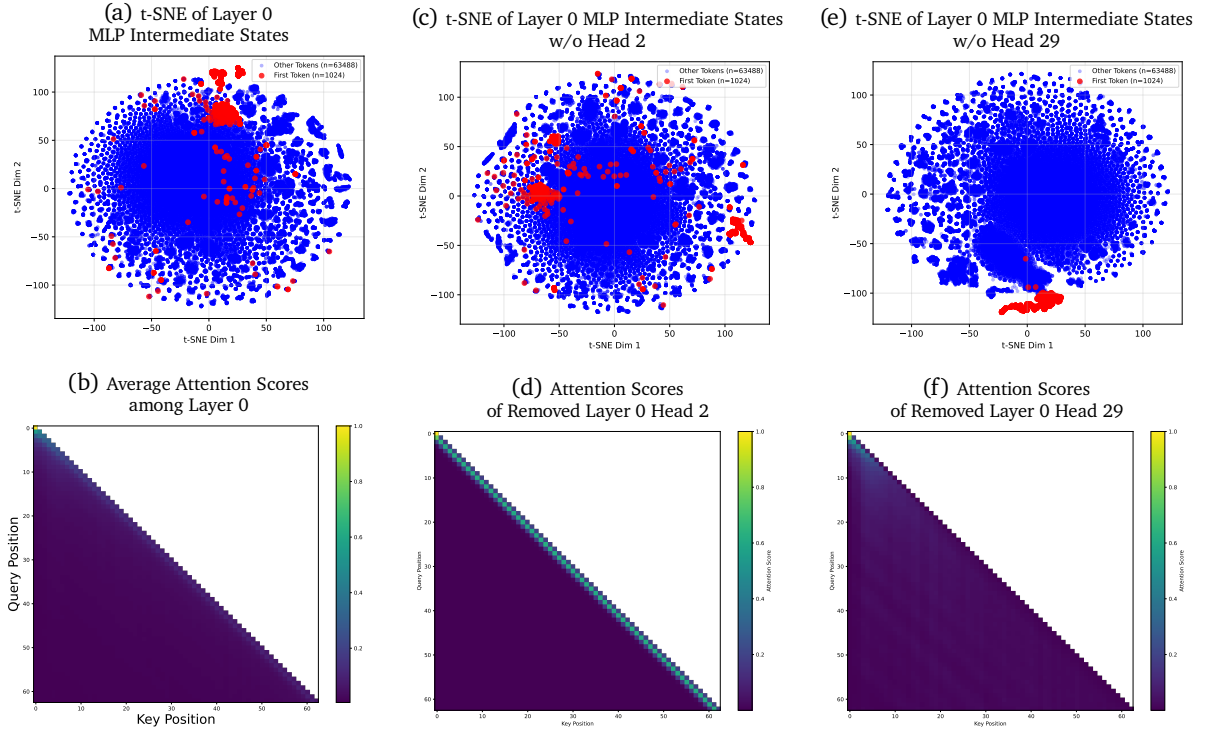


Figure 5: Visualization of intermediate MLP activations and attention scores in layer 0 of LLaMA3.1-8B. The [BOS] token has been removed. Several heads exhibit strong locality by primarily attending to neighboring tokens. Ablating individual heads does not weaken the clustering behavior at position zero; in fact, removing certain heads can even enhance it. This suggests that the effect arises from a complex, collaborative mechanism involving multiple attention heads.

To better formalize the model’s behavior in constructing a consistent and distinguishable representation for position-zero (P0), we begin by examining the pre-norm transformation applied to a hidden state vector $\mathbf{x} \in \mathbb{R}^d$, which precedes any downstream neural network module:

$$\text{Norm}(\mathbf{x}) = \frac{\mathbf{x}}{r(\mathbf{x})}, \quad (1)$$

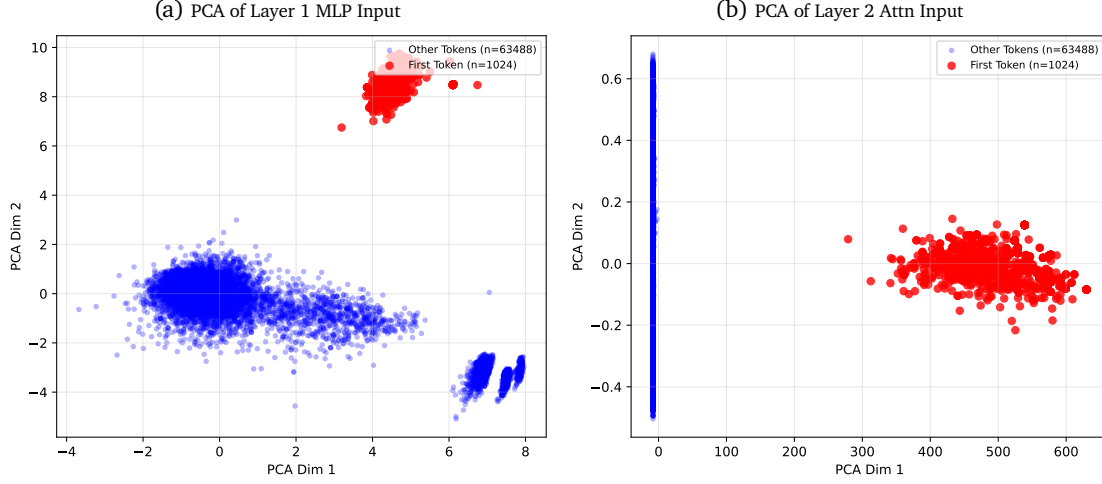


Figure 6: PCA of hidden states after the corresponding pre-layer normalization in LLaMA3.1-8B, with [BOS] token removed.

where the norm factor is defined as

$$r(\mathbf{x}) = \sqrt{\frac{1}{d} \mathbf{x}^\top \mathbf{x}}. \quad (2)$$

The Jacobian of this operation with respect to \mathbf{x} is given by:

$$\mathbf{J}_{\text{Norm}}(\mathbf{x}) = \frac{1}{r(\mathbf{x})} \mathbf{I} - \frac{1}{d} \frac{1}{r^3(\mathbf{x})} \mathbf{x} \mathbf{x}^\top. \quad (3)$$

Now consider a perturbation to the hidden state $\delta \mathbf{x} \ll \mathbf{x}$ induced by a backward update during training. This perturbation can be decomposed into components parallel and orthogonal to \mathbf{x} :

$$\delta \mathbf{x} = \delta \mathbf{x}_{\parallel} + \delta \mathbf{x}_{\perp}, \text{ where } \delta \mathbf{x}_{\parallel} = \alpha \mathbf{x}, \delta \mathbf{x}_{\perp} \cdot \mathbf{x} = 0. \quad (4)$$

The change in the normalized vector is approximately:

$$\text{Norm}(\mathbf{x} + \delta \mathbf{x}) - \text{Norm}(\mathbf{x}) \approx \mathbf{J}_{\text{Norm}}(\mathbf{x}) \delta \mathbf{x} = \frac{\delta \mathbf{x}_{\perp}}{r(\mathbf{x})}. \quad (5)$$

This expression leads to a key insight: when $r(\mathbf{x})$ is large, the effect of orthogonal perturbations $\delta \mathbf{x}_{\perp}$ on the normalized vector becomes proportionally smaller. Under the standard i.i.d. assumption on training data, gradient noise can be treated as approximately independent of the input. Thus, increasing the norm of \mathbf{x} reduces the sensitivity of its normalized direction to parameter updates.

4.2. Position Zero Identification Circuit

We now turn to how the model establishes the positional signature before the amplification phase. Empirically, the distinction of the first token is already visible in the hidden states after layer 0, where the position-zero representation is consistently pushed toward a relatively stable direction across inputs. This indicates that the model has already created a position-dependent asymmetry in the attention output prior to any strong MLP amplification. Additional evidence from Figure 6 confirms that this identification is already established before the MLP in layer 1, which corresponds to the model’s second transformer block.

As illustrated in Figure 5d, several attention heads in layer 0 exhibit strong locality. While this pattern might initially seem relevant to the emergence of the position-zero (PO) sink, head-level ablation studies suggest otherwise. In particular, the t-SNE visualization on head-level ablation [3] in Figure 5 shows that these local heads do not play a central role in producing the effect. Instead, the position-zero asymmetry arises from the

collective behavior of attention heads that distribute attention broadly and evenly across the sequence, following a statistically uniform averaging pattern. This effect appears to result from their coordinated interactions rather than from the influence of any individual head. Furthermore, as shown in Figure 5b, local heads contribute only marginally to the average attention scores. For these reasons, we focus our analysis on the aggregate behavior of the non-local attention heads.

Intuitively, under the causal constraint, uniform averaging induces an inherent asymmetry between position zero and all later positions. Tokens at all later positions aggregate diverse context vectors, which reduces the consistency of any shared directional component in their attention outputs. In contrast, position zero has access only to itself, so its attention output remains unmixed and preserves its direction more reliably. This asymmetry provides a clean signal that subsequent MLP sublayers can gate and amplify, eventually producing a stable P0 representation and the corresponding sink pattern.

Motivated by the empirical observation that uniform averaging heads play a crucial role in forming the P0 sink, we develop a simplified model to theoretically estimate the norm of the attention output. We assume that the input vectors to the attention module $\mathbf{x} = \mathbf{x}_0, \dots, \mathbf{x}_{l-1}$ have been normalized to unit norm due to pre-layer normalization, i.e., $\|\mathbf{x}_i\|_2 = 1$ for all i . Rather than modeling the detailed mechanism of attention, we abstract it as a weighted sum over value vectors $\mathbf{v}_0, \dots, \mathbf{v}_{l-1}$ using attention weights $\mathbf{p} = (p_0, \dots, p_{l-1})$.

Cone-based model of value vectors. As shown in Figure 4, the hidden states in LLMs exhibit clear directional bias and are far from isotropic. To capture this phenomenon, we model the value vectors \mathbf{v}_i as lying on a fixed-angle cone centered around a unit vector $\mathbf{u} \in \mathbb{R}^d$, where pre-norm normalization ensures $\|\mathbf{v}_i\|_2 = 1$. Figure 4 illustrates the cosine similarity structure. Each \mathbf{v}_i is assumed to have unit norm and to form a constant cosine similarity α with the cone axis \mathbf{u} . A convenient construction of such vectors is:

$$\mathbf{v}_i = \alpha \mathbf{u} + \sqrt{1 - \alpha^2} \mathbf{s}_i, \quad (6)$$

where each \mathbf{s}_i is a unit vector orthogonal to \mathbf{u} , sampled uniformly from the $(d - 1)$ -dimensional unit sphere, and independent across i .

Under this construction, it follows that:

$$\mathbb{E}[\mathbf{v}_i^\top \mathbf{v}_j] = \begin{cases} 1, & i = j, \\ \alpha^2, & i \neq j. \end{cases} \quad (7)$$

Attention output norm. Define the attention output of position $l - 1$ as the weighted sum \mathbf{c} :

$$\mathbf{c} = \sum_{i=0}^{l-1} p_i \mathbf{v}_i. \quad (8)$$

We aim to estimate its expected squared norm $\mathbb{E}[\|\mathbf{c}\|_2^2]$. First, expand the square:

$$\|\mathbf{c}\|_2^2 = \sum_i p_i^2 \|\mathbf{v}_i\|_2^2 + \sum_{i \neq j} p_i p_j \mathbf{v}_i^\top \mathbf{v}_j. \quad (9)$$

Taking expectation over \mathbf{v} conditioned on \mathbf{p} , and substituting in the known moments:

$$\begin{aligned} \mathbb{E}_{\mathbf{v}}[\|\mathbf{c}\|_2^2 \mid \mathbf{p}] &= \sum_i p_i^2 \cdot 1 + \sum_{i \neq j} p_i p_j \cdot \alpha^2 \\ &= \sum_i p_i^2 + \alpha^2 \left(1 - \sum_i p_i^2 \right) \\ &= \alpha^2 + (1 - \alpha^2) \sum_i p_i^2. \end{aligned} \quad (10)$$

Finally, taking expectation over \mathbf{p} gives:

$$\mathbb{E}[\|\mathbf{c}\|_2^2] = \alpha^2 + (1 - \alpha^2) \mathbb{E} \left[\sum_i p_i^2 \right]. \quad (11)$$

Token Index	0	1	2	4	8	16	32	64
Llama-3.1-8B	0.87	0.82	0.79	0.73	0.66	0.63	0.61	0.59
Llama-3.2-1B	1.04	1.03	0.98	0.96	0.91	0.90	0.88	0.87
Llama-3.2-3B	1.37	1.29	1.21	1.17	1.11	1.10	1.07	1.05

Table 2: ℓ_2 Norm of Layer 0 Attention Output, w/o [BOS]

Token Repeat Time (n)	n=2	n=3	n=4
Llama-3 Tokenizer	2.01×10^{-4}	6.10×10^{-5}	2.90×10^{-5}
Mistral-v0.3 Tokenizer	4.12×10^{-3}	6.28×10^{-4}	5.90×10^{-5}
Qwen3 Tokenizer	4.52×10^{-3}	6.88×10^{-4}	6.00×10^{-5}

Table 3: Proportion of n -grams in which the same token appears n times consecutively, measured under different tokenizers on a subset of FineWeb-Edu 10B dataset [11]. This analysis confirms that repeated-token patterns are rare and are unlikely to introduce out-of-distribution artifacts that could confound our findings.

While the full distribution of attention weights \mathbf{p} is difficult to characterize analytically, empirical observations suggest that attention tends to be sparse across positions [21]. This sparsity implies that the second-order statistic $\mathbb{E}[\sum_i p_i^2]$ typically decreases monotonically as the sequence length l increases. This theoretical behavior aligns with our empirical finding that the ℓ_2 norm of the attention output decreases with increasing sequence length l , as shown in Table 2.

Specifically, to ensure that our assumption is not confounded by the out-of-distribution effect caused by repeated contiguous tokens, as discussed in Section 3, we verify the proportion of n -grams in which the same token appears n times consecutively under different tokenizers. The results, summarized in Table 3, show that such occurrences are rare across common tokenizers. This confirms that the simultaneous occurrence of identical tokens at both position zero and position one is highly unlikely in practice, which further justifies that training without a [BOS] token does not introduce significant ambiguity.

Leveraging this distributional asymmetry, the model is able to cluster the hidden states at position zero using only the up-projection components of the MLP, without incorporating any semantic information. The activation function serves as a gating mechanism, allowing the subsequent MLP layer to transform the resulting vector into a stable and position-specific representation. Together, these components constitute what we refer to as the **P0-Sink Circuit**.

5. How P0 Sink Emerges in Pre-training

We have shown that a two-layer circuit is sufficient to induce a persistent position-zero sink that propagates to deeper layers. This naturally leads to the question: why do some models fail to form such a representation by the second layer? To explore this, we analyze training traces from a 30B-A3B MoE model trained from scratch². These traces offer insights into both the emergence and stabilization of the position-zero representation over the course of training.

For clarity, we divide the model’s training process into three distinct stages. In the **early stage**, a P0-Sink Circuit emerges in the middle layers of the model. However, this signal gradually fades and is replaced by a broader sink pattern that spans multiple positions. In the **transition stage**, the model temporarily relies on alternative tokens (e.g. position one) to form shallow, single-position sinks. These progressively shift and stabilize into a consistent position-zero sink within the shallow layers. The **final stage**, which we do not

²The model architecture and optimization hyperparameters follow those described in Qwen3 technical report [17], with an enhanced version of Wanjuan-CC as the pretraining corpus [13].

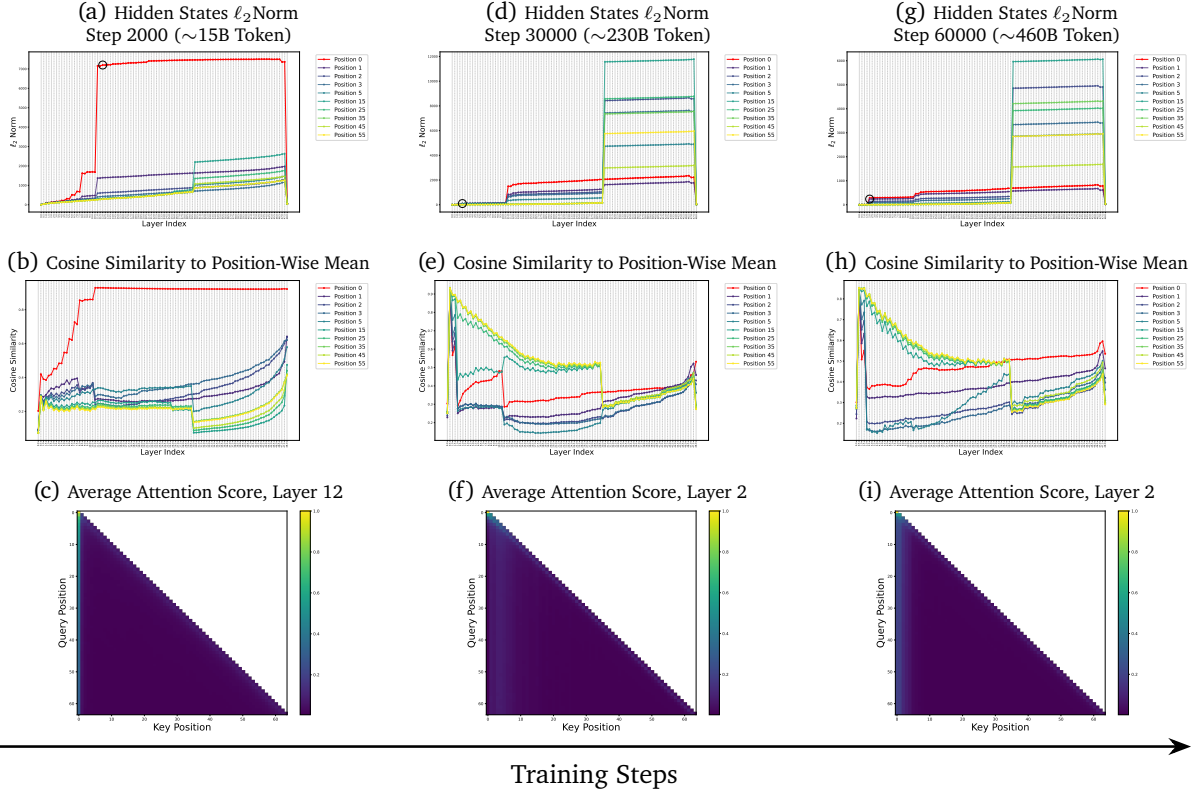


Figure 7: Early-stage training statistics showing a rise in P0 ℓ_2 norms and sink emergence in middle layers. As training continues, these fade into broader multi-position sinks. **Position-wise Mean** is computed across samples per position and layer.

elaborate on in this work, is characterized by a fixed sink configuration that remains stable throughout the remainder of training.

5.1. Early Stage

As shown in Figure 7, the P0-Sink Circuit emerges within the first 15B training tokens and initially appears in the middle layers of the network. This early emergence suggests that the mechanism benefits training by providing a favorable local optimum under language modeling objectives. While the P0 behavior remains the most prominent and stable, a similar but weaker pattern is also observed at position one. This observation supports our earlier analysis in Equation 11, which identifies relative averaging and position mixing, rather than explicit position-specific priors, as the underlying drivers of the sink effect.

This understanding also provides a concrete explanation for the drop in **Sink Rate** observed by Barbero et al. [2] when removing the [BOS] token from pretrained models. As defined by Gu et al. [8], the Sink Rate measures the proportion of attention heads and layers that allocate an average attention score above a moderate threshold ε to a given token. [BOS], the embedding vector of [BOS] facilitates early-layer sinks directly leading to elevated Sink Rates in shallow layers. When [BOS] is removed, models require deeper layers to build the **P0-Sink Circuit**, especially in the early stages of training where token exposure is limited. This results in a lower measured Sink Rate across the network.

However, such effects are no longer observed in more recent models. As modern LLMs are typically trained on significantly larger corpora, as stated in their official reports, even small models such as LLaMA-1B (shown in Figure 10) are able to develop robust sink circuits within the first few layers. As a result, the absence of a [BOS] token has a diminishing impact on the observed Sink Rate.

At around 230B training tokens, the original P0 sink begins to fade. In its place, the model develops a broader sink pattern starting from layer 2, where attention is consistently concentrated on the early part of the input sequence. This pattern typically involves the first several tokens. Remarkably, this behavior

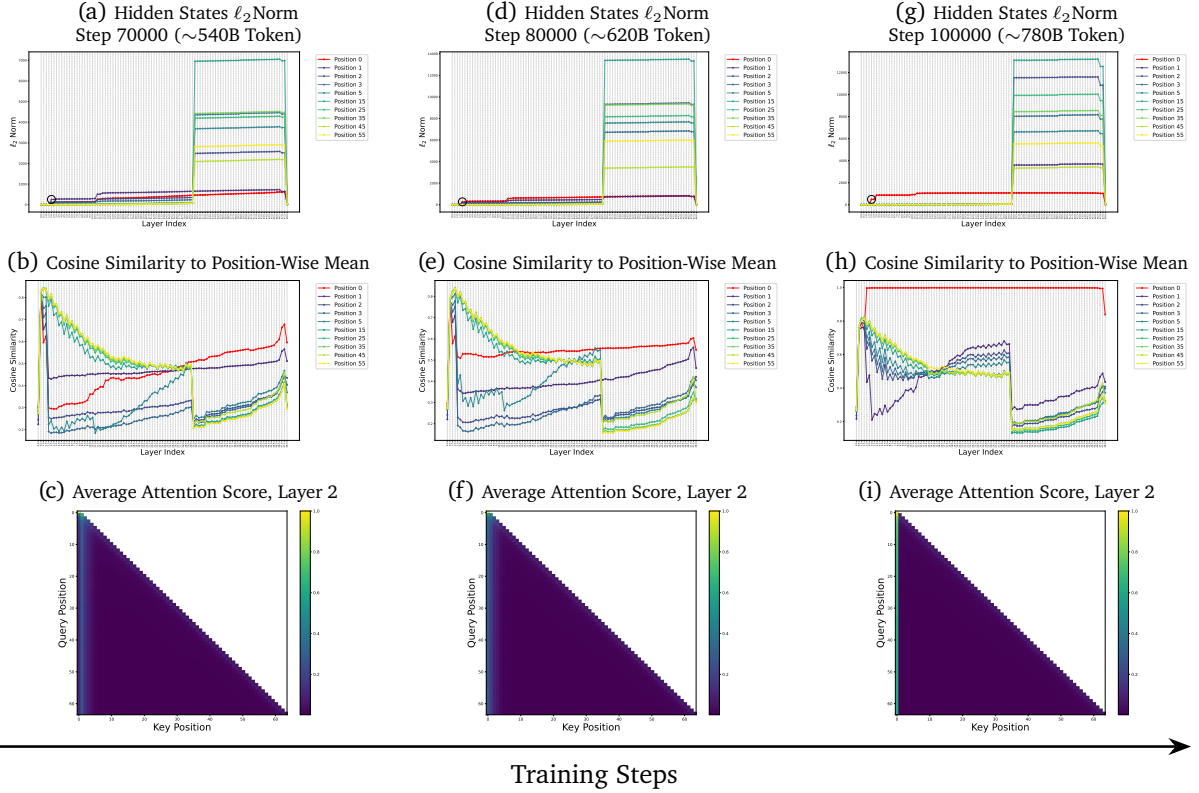


Figure 8: Visualization of statistics during the Transitional Stage. The model temporarily shifts its sink center to position 1 as a transitional phase, before establishing a stable position-zero sink by forming an identification circuit for position 0.

persists through all subsequent layers and remains stable until at least 460B tokens. In this stage, the attention pattern closely mirrors those observed in StreamingLLM [16], where the initial tokens are expected to function as persistent context anchors. The structural similarity suggests that this broad-spectrum sink may serve a similar role, facilitating stable context accumulation in long sequences and supporting efficient autoregressive processing.

During training, we also observe a distinct phenomenon in the deeper layers. After layer 30, certain activations become abnormally large and exhibit clear position-dependent patterns. However, as shown in the visualizations in Appendix B, the corresponding attention scores remain largely unaffected. Since this effect does not directly impact the attention mechanism and falls outside the main scope of our study, we leave a detailed analysis to future work and restrict our focus to the earlier layers, where the sink mechanism more clearly emerges.

5.2. Transitional Stage

After a prolonged phase dominated by a broad-spectrum sink pattern, the influence of the initial position-zero circuit gradually diminishes. One possible explanation is that the earlier layers begin to transition into a form of sink-based attention that enables head-level gating control, as discussed by Sandoval-Segura et al. [15]. The model subsequently shifts its sink center from position zero to position one. Notably, this new sink emerges earlier in the network, beginning at layer 2, as illustrated in Figure 8c. In this context, we use the term *sink center* to refer to the token position whose hidden states are most consistently clustered and reinforced across layers, thereby serving as a persistent anchor for attention throughout the model.

As shown in Figure 8, the model attempts to identify commonalities among position-one tokens and cluster their hidden states into a consistent representation, thereby establishing a stable sink at position one. However, this configuration proves to be transient. After only a modest number of additional training steps, the sink shifts back to position zero and persists there through later stages of training.

This shift can be explained by the structural asymmetry formalized in Equation 11. Under causal attention, position zero is inherently more invariant to input variation, as it attends only to itself. In contrast, position one aggregates signals from both itself and position zero, resulting in a representation that is more context-dependent and therefore more difficult to align across different inputs. This structural advantage renders position zero more suitable for amplification into a stable attention sink. As a result, the model eventually reestablishes the position-zero sink, which then remains consistent throughout the remainder of training.

5.3. Implications and Applications

Based on the observed phenomena associated with the position-zero sink, we hypothesize that the stage at which this sink circuit stabilizes, whether it is the early stage, the transitional stage, or the final stage, can serve as an indicator of the model’s pretraining convergence status. It is important to note that reaching a later stage does not necessarily imply stronger performance. Instead, the sink stage reflects the model’s position within the pretraining trajectory. If post-training is initiated while the model remains in an earlier sink stage, continued pretraining may lead to improved downstream performance. We provide further analysis in Appendix C.

6. Conclusion

In this work, we study how position-zero attention sinks arise and persist in modern large language models. We show that while the [BOS] token contributes to sink behavior in shallow layers for models trained with it, a robust position-zero sink persists in deeper layers even after removing [BOS], indicating that the sink phenomenon is not reducible to token embeddings.

We further identify a simple and generalizable two-block transformer circuit that enables the model to recognize position zero tokens and amplify the ℓ_2 norm of its hidden state, thereby stabilizing the sink pattern across layers. By tracing training dynamics in a 30B-parameter model with 3B activated parameters trained from scratch, we show that this **PO-Sink Circuit** emerges early and becomes concentrated in the first two layers over time.

These findings reveal the mechanism behind attention sink emergence and offer a diagnostic signal for estimating training stage and convergence. More broadly, they highlight implicit architectural biases in transformers and suggest directions for improving interpretability, efficiency, and stability in future designs.

Acknowledgement

We thank Tianyang Lin and Demin Song for providing model checkpoints used in our analysis.

References

- [1] Jimmy Lei Ba, Jamie Ryan Kiros, and Geoffrey E. Hinton. Layer normalization, 2016. URL <https://arxiv.org/abs/1607.06450>. 4.1
- [2] Federico Barbero, Álvaro Arroyo, Xiangming Gu, Christos Perivolaropoulos, Michael Bronstein, Petar Veličković, and Razvan Pascanu. Why do llms attend to the first token?, 2025. URL <https://arxiv.org/abs/2504.02732>. 2, 3, 5.1
- [3] T. Tony Cai and Rong Ma. Theoretical foundations of t-sne for visualizing high-dimensional clustered data, 2022. URL <https://arxiv.org/abs/2105.07536>. 4.2
- [4] Nicola Cancedda. Spectral filters, dark signals, and attention sinks, 2024. URL <https://arxiv.org/abs/2402.09221>. 1, 2, 3
- [5] Zhuoming Chen, Ranajoy Sadhukhan, Zihao Ye, Yang Zhou, Jianyu Zhang, Niklas Nolte, Yuandong Tian, Matthijs Douze, Leon Bottou, Zhihao Jia, and Beidi Chen. Magicpig: Lsh sampling for efficient llm generation, 2024. URL <https://arxiv.org/abs/2410.16179>. 1
- [6] Borjan Geshkovski, Cyril Letrouit, Yury Polyanskiy, and Philippe Rigollet. The emergence of clusters in self-attention dynamics, 2024. URL <https://arxiv.org/abs/2305.05465>. 2
- [7] Aaron Grattafiori, Abhimanyu Dubey, Abhinav Jauhri, Abhinav Pandey, Abhishek Kadian, Ahmad Al-Dahle, Aiesha Letman, Akhil Mathur, Alan Schelten, Alex Vaughan, Amy Yang, Angela Fan, Anirudh Goyal, Anthony Hartshorn, Aobo Yang, Archi Mitra, Archie Sravankumar, Artem Korenev, Arthur Hinsvark, Arun Rao, Aston Zhang, Aurelien Rodriguez, Austen Gregerson, Ava Spataru, Baptiste Roziere, Bethany Biron, Binh Tang, Bobbie Chern, Charlotte Caucheteux, Chaya Nayak, Chloe Bi, Chris Marra, Chris McConnell, Christian Keller, Christophe Touret, Chunyang Wu, Corinne Wong, Cristian Canton Ferrer, Cyrus Nikolaidis, Damien Allonsius, Daniel Song, Danielle Pintz, Danny Livshits, Danny Wyatt, David Esiobu, Dhruv Choudhary, Dhruv Mahajan, Diego Garcia-Olano, Diego Perino, Dieuwke Hupkes, Egor Lakomkin, Ehab AlBadawy, Elina Lobanova, Emily Dinan, Eric Michael Smith, Filip Radenovic, Francisco Guzmán, Frank Zhang, Gabriel Synnaeve, Gabrielle Lee, Georgia Lewis Anderson, Govind Thattai, Graeme Nail, Gregoire Mialon, Guan Pang, Guillem Cucurell, Hailey Nguyen, Hannah Korevaar, Hu Xu, Hugo Touvron, Iliyan Zarov, Imanol Arrieta Ibarra, Isabel Kloumann, Ishan Misra, Ivan Evtimov, Jack Zhang, Jade Copet, Jaewon Lee, Jan Geffert, Jana Vranes, Jason Park, Jay Mahadeokar, Jeet Shah, Jelmer van der Linde, Jennifer Billock, Jenny Hong, Jenya Lee, Jeremy Fu, Jianfeng Chi, Jianyu Huang, Jiawen Liu, Jie Wang, Jiecao Yu, Joanna Bitton, Joe Spisak, Jongsoo Park, Joseph Rocca, Joshua Johnstun, Joshua Saxe, Junteng Jia, Kalyan Vasuden Alwala, Karthik Prasad, Kartikeya Upasani, Kate Plawiak, Ke Li, Kenneth Heafield, Kevin Stone, Khalid El-Arini, Krithika Iyer, Kshitiz Malik, Kuenley Chiu, Kunal Bhalla, Kushal Lakhotia, Lauren Rantala-Yearly, Laurens van der Maaten, Lawrence Chen, Liang Tan, Liz Jenkins, Louis Martin, Lovish Madaan, Lubo Malo, Lukas Blecher, Lukas Landzaat, Luke de Oliveira, Madeline Muzzi, Mahesh Pasupuleti, Mannat Singh, Manohar Paluri, Marcin Kardas, Maria Tsimpoukelli, Mathew Oldham, Mathieu Rita, Maya Pavlova, Melanie Kambadur, Mike Lewis, Min Si, Mitesh Kumar Singh, Mona Hassan, Naman Goyal, Narjes Torabi, Nikolay Bashlykov, Nikolay Bogoychev, Niladri Chatterji, Ning Zhang, Olivier Duchenne, Onur Çelebi, Patrick Alrassy, Pengchuan Zhang, Pengwei Li, Petar Vasic, Peter Weng, Prajjwal Bhargava, Pratik Dubal, Praveen Krishnan, Punit Singh Koura, Puxin Xu, Qing He, Qingxiao Dong, Ragavan Srinivasan, Raj Ganapathy, Ramon Calderer, Ricardo Silveira Cabral, Robert Stojnic, Roberta Raileanu, Rohan Maheswari, Rohit Girdhar, Rohit Patel, Romain Sauvestre, Ronnie Polidoro, Roshan Sumbaly, Ross Taylor, Ruan Silva, Rui Hou, Rui Wang, Saghar Hosseini, Sahana Chennabasappa, Sanjay Singh, Sean Bell, Seohyun Sonia Kim, Sergey Edunov, Shaoliang Nie, Sharan Narang, Sharath Rapparthi, Sheng Shen, Shengye Wan, Shruti Bhosale, Shun Zhang, Simon Vandenhende, Soumya Batra, Spencer Whitman, Sten Sootla, Stephane Collot, Suchin Gururangan, Sydney Borodinsky, Tamar Herman, Tara Fowler, Tarek Sheasha, Thomas Georgiou, Thomas Scialom, Tobias Speckbacher, Todor Mihaylov, Tong Xiao, Ujjwal Karn, Vedanuj Goswami, Vibhor Gupta, Vignesh Ramanathan, Viktor Kerkez, Vincent Gonguet, Virginie Do, Vish Vogeti, Vitor Albiero, Vladan Petrovic, Weiwei Chu, Wenhan Xiong, Wenyin Fu, Whitney Meers, Xavier Martinet, Xiaodong Wang, Xiaofang Wang, Xiaoqing Ellen Tan, Xide Xia, Xinfeng Xie, Xuchao Jia, Xuewei Wang, Yaelle Goldschlag, Yashesh Gaur, Yasmine Babaei, Yi Wen, Yiwen Song, Yuchen Zhang, Yue Li, Yuning Mao, Zacharie Delpierre Coudert, Zheng Yan, Zhengxing Chen, Zoe

Papakipos, Aaditya Singh, Aayushi Srivastava, Abha Jain, Adam Kelsey, Adam Shajnfeld, Adithya Gangidi, Adolfo Victoria, Ahuva Goldstand, Ajay Menon, Ajay Sharma, Alex Boesenberg, Alexei Baevski, Allie Feinstein, Amanda Kallet, Amit Sangani, Amos Teo, Anam Yunus, Andrei Lupu, Andres Alvarado, Andrew Caples, Andrew Gu, Andrew Ho, Andrew Poulton, Andrew Ryan, Ankit Ramchandani, Annie Dong, Annie Franco, Anuj Goyal, Aparajita Saraf, Arkabandhu Chowdhury, Ashley Gabriel, Ashwin Bharambe, Assaf Eisenman, Azadeh Yazdan, Beau James, Ben Maurer, Benjamin Leonhardi, Bernie Huang, Beth Loyd, Beto De Paola, Bhargavi Paranjape, Bing Liu, Bo Wu, Boyu Ni, Braden Hancock, Bram Wasti, Brandon Spence, Brani Stojkovic, Brian Gamido, Britt Montalvo, Carl Parker, Carly Burton, Catalina Mejia, Ce Liu, Changan Wang, Changkyu Kim, Chao Zhou, Chester Hu, Ching-Hsiang Chu, Chris Cai, Chris Tindal, Christoph Feichtenhofer, Cynthia Gao, Damon Civin, Dana Beaty, Daniel Kreymer, Daniel Li, David Adkins, David Xu, Davide Testuggine, Delia David, Devi Parikh, Diana Liskovich, Didem Foss, Ding Kang Wang, Duc Le, Dustin Holland, Edward Dowling, Eissa Jamil, Elaine Montgomery, Eleonora Presani, Emily Hahn, Emily Wood, Eric-Tuan Le, Erik Brinkman, Esteban Arcaute, Evan Dunbar, Evan Smothers, Fei Sun, Felix Kreuk, Feng Tian, Filippos Kokkinos, Firat Ozgenel, Francesco Caggioni, Frank Kanayet, Frank Seide, Gabriela Medina Florez, Gabriella Schwarz, Gada Badeer, Georgia Swee, Gil Halpern, Grant Herman, Grigory Sizov, Guangyi, Zhang, Guna Lakshminarayanan, Hakan Inan, Hamid Shojanazeri, Han Zou, Hannah Wang, Hanwen Zha, Haroun Habeeb, Harrison Rudolph, Helen Suk, Henry Aspegren, Hunter Goldman, Hongyuan Zhan, Ibrahim Damla, Igor Molybog, Igor Tufanov, Ilias Leontiadis, Irina-Elena Veliche, Itai Gat, Jake Weissman, James Geboski, James Kohli, Janice Lam, Japhet Asher, Jean-Baptiste Gaya, Jeff Marcus, Jeff Tang, Jennifer Chan, Jenny Zhen, Jeremy Reizenstein, Jeremy Teboul, Jessica Zhong, Jian Jin, Jingyi Yang, Joe Cummings, Jon Carvill, Jon Shepard, Jonathan McPhie, Jonathan Torres, Josh Ginsburg, Junjie Wang, Kai Wu, Kam Hou U, Karan Saxena, Kartikay Khandelwal, Katayoun Zand, Kathy Matosich, Kaushik Veeraraghavan, Kelly Michelena, Keqian Li, Kiran Jagadeesh, Kun Huang, Kunal Chawla, Kyle Huang, Lailin Chen, Lakshya Garg, Lavender A, Leandro Silva, Lee Bell, Lei Zhang, Liangpeng Guo, Licheng Yu, Liron Moshkovich, Luca Wehrstedt, Madian Khabsa, Manav Avalani, Manish Bhatt, Martynas Mankus, Matan Hasson, Matthew Lennie, Matthias Reso, Maxim Groshev, Maxim Naumov, Maya Lathi, Meghan Keneally, Miao Liu, Michael L. Seltzer, Michal Valko, Michelle Restrepo, Mihir Patel, Mik Vyatskov, Mikayel Samvelyan, Mike Clark, Mike Macey, Mike Wang, Miquel Jubert Hermoso, Mo Metanat, Mohammad Rastegari, Munish Bansal, Nandhini Santhanam, Natascha Parks, Natasha White, Navyata Bawa, Nayan Singhal, Nick Egebo, Nicolas Usunier, Nikhil Mehta, Nikolay Pavlovich Laptev, Ning Dong, Norman Cheng, Oleg Chernoguz, Olivia Hart, Omkar Salpekar, Ozlem Kalinli, Parkin Kent, Parth Parekh, Paul Saab, Pavan Balaji, Pedro Rittner, Philip Bontrager, Pierre Roux, Piotr Dollar, Polina Zvyagina, Prashant Ratanchandani, Pritish Yuvraj, Qian Liang, Rachad Alao, Rachel Rodriguez, Rafi Ayub, Raghotham Murthy, Raghu Nayani, Rahul Mitra, Rangaprabhu Parthasarathy, Raymond Li, Rebekkah Hogan, Robin Battey, Rocky Wang, Russ Howes, Ruty Rinott, Sachin Mehta, Sachin Siby, Sai Jayesh Bondu, Samyak Datta, Sara Chugh, Sara Hunt, Sargun Dhillon, Sasha Sidorov, Satadru Pan, Saurabh Mahajan, Saurabh Verma, Seiji Yamamoto, Sharadh Ramaswamy, Shaun Lindsay, Shaun Lindsay, Sheng Feng, Shenghao Lin, Shengxin Cindy Zha, Shishir Patil, Shiva Shankar, Shuqiang Zhang, Shuqiang Zhang, Sinong Wang, Sneha Agarwal, Soji Sajuyigbe, Soumith Chintala, Stephanie Max, Stephen Chen, Steve Kehoe, Steve Satterfield, Sudarshan Govindaprasad, Sumit Gupta, Summer Deng, Sungmin Cho, Sunny Virk, Suraj Subramanian, Sy Choudhury, Sydney Goldman, Tal Remez, Tamar Glaser, Tamara Best, Thilo Koehler, Thomas Robinson, Tianhe Li, Tianjun Zhang, Tim Matthews, Timothy Chou, Tzook Shaked, Varun Vontimitta, Victoria Ajayi, Victoria Montanez, Vijai Mohan, Vinay Satish Kumar, Vishal Mangla, Vlad Ionescu, Vlad Poenaru, Vlad Tiberiu Mihailescu, Vladimir Ivanov, Wei Li, Wenchen Wang, Wenwen Jiang, Wes Bouaziz, Will Constable, Xiaocheng Tang, Xiaoqian Wu, Xiaolan Wang, Xilun Wu, Xinbo Gao, Yaniv Kleinman, Yanjun Chen, Ye Hu, Ye Jia, Ye Qi, Yenda Li, Yilin Zhang, Ying Zhang, Yossi Adi, Youngjin Nam, Yu, Wang, Yu Zhao, Yuchen Hao, Yundi Qian, Yunlu Li, Yuzi He, Zach Rait, Zachary DeVito, Zef Rosnbrick, Zhaoduo Wen, Zhenyu Yang, Zhiwei Zhao, and Zhiyu Ma. The llama 3 herd of models, 2024. URL <https://arxiv.org/abs/2407.21783>. 1, 3

- [8] Xiangming Gu, Tianyu Pang, Chao Du, Qian Liu, Fengzhuo Zhang, Cunxiao Du, Ye Wang, and Min Lin. When attention sink emerges in language models: An empirical view, 2025. URL <https://arxiv.org/abs/2410.10781>. 1, 2, 3, 5.1
- [9] Tianyu Guo, Druv Pai, Yu Bai, Jiantao Jiao, Michael Jordan, and Song Mei. Active-dormant attention heads: Mechanistically demystifying extreme-token phenomena in LLMs, 2025. URL <https://openreview.net/forum?id=uEPRY2XAEs>. 2

- [10] Chi Han, Qifan Wang, Hao Peng, Wenhan Xiong, Yu Chen, Heng Ji, and Sinong Wang. LM-infinite: Zero-shot extreme length generalization for large language models. In Kevin Duh, Helena Gomez, and Steven Bethard, editors, *Proceedings of the 2024 Conference of the North American Chapter of the Association for Computational Linguistics: Human Language Technologies (Volume 1: Long Papers)*, pages 3991–4008, Mexico City, Mexico, June 2024. Association for Computational Linguistics. doi: 10.18653/v1/2024-naacl-long.222. URL <https://aclanthology.org/2024.naacl-long.222/>. 1
- [11] Anton Lozhkov, Loubna Ben Allal, Leandro von Werra, and Thomas Wolf. Fineweb-edu: the finest collection of educational content, 2024. URL <https://huggingface.co/datasets/HuggingFaceFW/fineweb-edu>. 1, 3
- [12] Team OLMo, Pete Walsh, Luca Soldaini, Dirk Groeneveld, Kyle Lo, Shane Arora, Akshita Bhagia, Yuling Gu, Shengyi Huang, Matt Jordan, Nathan Lambert, Dustin Schwenk, Oyvind Tafjord, Taira Anderson, David Atkinson, Faeze Brahman, Christopher Clark, Pradeep Dasigi, Nouha Dziri, Allyson Ettinger, Michal Guerquin, David Heineman, Hamish Ivison, Pang Wei Koh, Jiacheng Liu, Saumya Malik, William Merrill, Lester James V. Miranda, Jacob Morrison, Tyler Murray, Crystal Nam, Jake Poznanski, Valentina Pyatkin, Aman Rangapur, Michael Schmitz, Sam Skjonsberg, David Wadden, Christopher Wilhelm, Michael Wilson, Luke Zettlemoyer, Ali Farhadi, Noah A. Smith, and Hannaneh Hajishirzi. 2 olmo 2 furious, 2025. URL <https://arxiv.org/abs/2501.00656>. 3
- [13] Jiantao Qiu, Haijun Lv, Zhenjiang Jin, Rui Wang, Wenchang Ning, Jia Yu, ChaoBin Zhang, Zhenxiang Li, Pei Chu, Yuan Qu, Jin Shi, Lindong Lu, Runyu Peng, Zhiyuan Zeng, Huanze Tang, Zhikai Lei, Jiawei Hong, Keyu Chen, Zhaoye Fei, Ruiliang Xu, Wei Li, Zhongying Tu, Lin Dahua, Yu Qiao, Hang Yan, and Conghui He. Wanjuan-cc: A safe and high-quality open-sourced english webtext dataset, 2024. URL <https://arxiv.org/abs/2402.19282>. 2
- [14] Qwen, :, An Yang, Baosong Yang, Beichen Zhang, Binyuan Hui, Bo Zheng, Bowen Yu, Chengyuan Li, Dayiheng Liu, Fei Huang, Haoran Wei, Huan Lin, Jian Yang, Jianhong Tu, Jianwei Zhang, Jianxin Yang, Jiayi Yang, Jingren Zhou, Junyang Lin, Kai Dang, Keming Lu, Keqin Bao, Kexin Yang, Le Yu, Mei Li, Mingfeng Xue, Pei Zhang, Qin Zhu, Rui Men, Runji Lin, Tianhao Li, Tianyi Tang, Tingyu Xia, Xingzhang Ren, Xuancheng Ren, Yang Fan, Yang Su, Yichang Zhang, Yu Wan, Yuqiong Liu, Zeyu Cui, Zhenru Zhang, and Zihan Qiu. Qwen2.5 technical report, 2025. URL <https://arxiv.org/abs/2412.15115>. 3
- [15] Pedro Sandoval-Segura, Xijun Wang, Ashwinee Panda, Micah Goldblum, Ronen Basri, Tom Goldstein, and David Jacobs. Identifying and evaluating inactive heads in pretrained llms, 2025. URL <https://arxiv.org/abs/2504.03889>. 2, 3, 5.2
- [16] Guangxuan Xiao, Yuandong Tian, Beidi Chen, Song Han, and Mike Lewis. Efficient streaming language models with attention sinks, 2024. URL <https://arxiv.org/abs/2309.17453>. 1, 5.1
- [17] An Yang, Anfeng Li, Baosong Yang, Beichen Zhang, Binyuan Hui, Bo Zheng, Bowen Yu, Chang Gao, Chengen Huang, Chenxu Lv, Chujie Zheng, Dayiheng Liu, Fan Zhou, Fei Huang, Feng Hu, Hao Ge, Haoran Wei, Huan Lin, Jialong Tang, Jian Yang, Jianhong Tu, Jianwei Zhang, Jianxin Yang, Jiayi Yang, Jing Zhou, Jingren Zhou, Junyang Lin, Kai Dang, Keqin Bao, Kexin Yang, Le Yu, Lianghao Deng, Mei Li, Mingfeng Xue, Mingze Li, Pei Zhang, Peng Wang, Qin Zhu, Rui Men, Ruize Gao, Shixuan Liu, Shuang Luo, Tianhao Li, Tianyi Tang, Wenbiao Yin, Xingzhang Ren, Xinyu Wang, Xinyu Zhang, Xuancheng Ren, Yang Fan, Yang Su, Yichang Zhang, Yinger Zhang, Yu Wan, Yuqiong Liu, Zekun Wang, Zeyu Cui, Zhenru Zhang, Zhipeng Zhou, and Zihan Qiu. Qwen3 technical report, 2025. URL <https://arxiv.org/abs/2505.09388>. 3, 2
- [18] Zhongzhi Yu, Zheng Wang, Yonggan Fu, Huihong Shi, Khalid Shaikh, and Yingyan Celine Lin. Unveiling and harnessing hidden attention sinks: Enhancing large language models without training through attention calibration, 2024. URL <https://arxiv.org/abs/2406.15765>. 1
- [19] Biao Zhang and Rico Sennrich. Root mean square layer normalization, 2019. URL <https://arxiv.org/abs/1910.07467>. 4.1
- [20] Stephen Zhang, Mustafa Khan, and Vardan Papayan. Attention sinks: A ‘catch, tag, release’ mechanism for embeddings, 2025. URL <https://arxiv.org/abs/2502.00919>. 2

- [21] Nicolas Zucchet, Francesco D’Angelo, Andrew Kyle Lampinen, and Stephanie C.Y. Chan. The emergence of sparse attention: impact of data distribution and benefits of repetition. In *The Thirty-ninth Annual Conference on Neural Information Processing Systems*, 2025. URL <https://openreview.net/forum?id=jMhRbV47pS>. 4.2

A. Dataset and Setup

Unless otherwise specified (e.g., Table 3), all experiments in this paper are conducted on a 10B-token subset of the FineWeb-Edu dataset, specifically using the first 1024 samples from the first .parquet file, with a maximum sequence length of 64.

B. Checkpoint Attention Heatmap

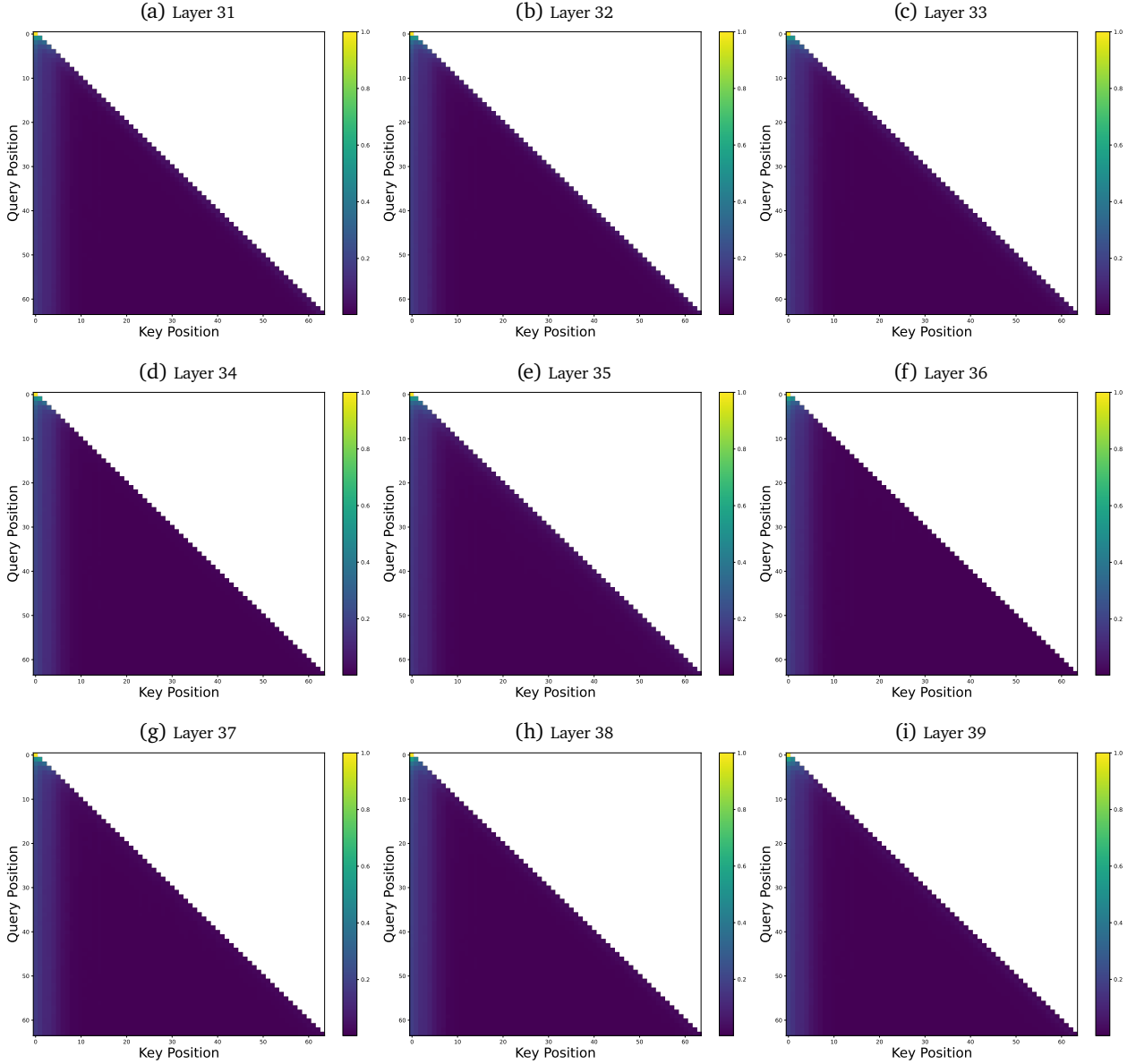


Figure 9: Mean attention maps from selected deep layers at step 30000. Notably, large ℓ_2 -norm hidden states at non-P0 positions do not noticeably affect the attention patterns, suggesting limited relevance to the sink mechanism. We leave further investigation to future work.

C. Recent LLM’s Statistics

C.1. LLaMA-3 Series Analysis

The LLaMA-3 family exhibits behaviors consistent with those discussed in the main text, and we omit further elaboration here for brevity.

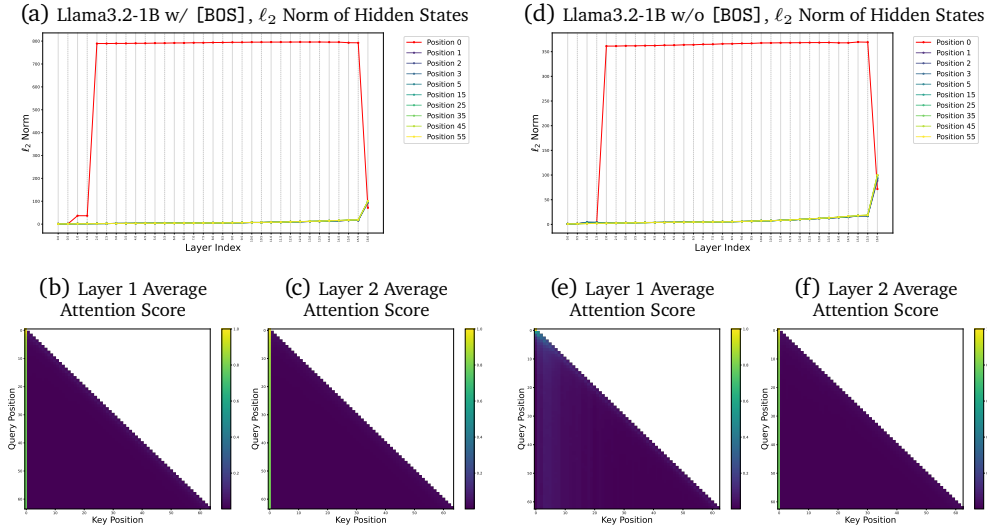


Figure 10: Layer-wise ℓ_2 norm of hidden states and attention score heat maps in LLaMA3.2-1B. Half-integer indices correspond to the output of attention modules after residual connection. Removing the [BOS] token eliminates the layer-1 attention sink and its associated ℓ_2 norm amplification. However, due to renewed norm growth before layer 2, a position-zero (P0) sink re-emerges in the attention maps even in the absence of the [BOS] token.

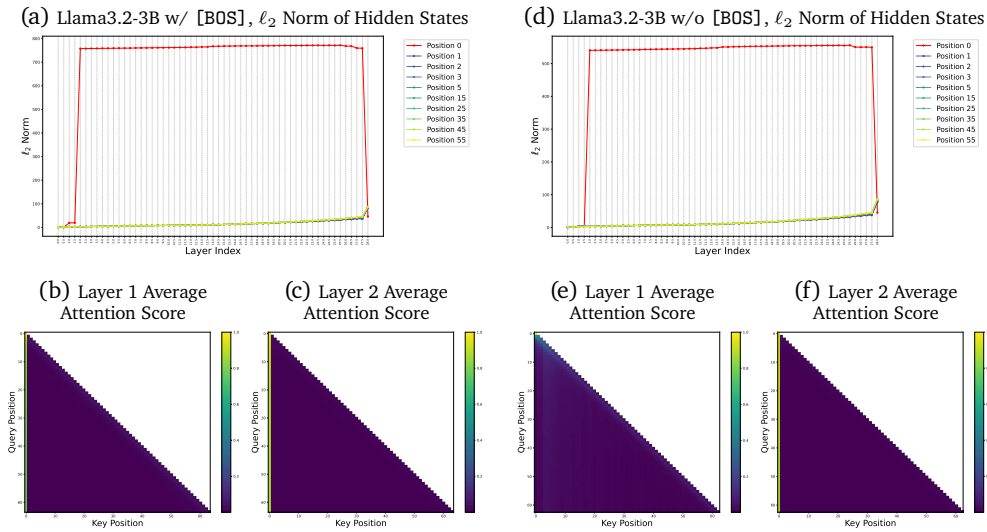


Figure 11: Layer-wise ℓ_2 norm of hidden states and attention score heat maps in LLaMA3.2-3B. Half-integer indices correspond to the output of attention modules after residual connection. Removing the [BOS] token eliminates the layer-1 attention sink and its associated ℓ_2 norm amplification. However, due to renewed norm growth before layer 2, a position-zero (P0) sink re-emerges in the attention maps even in the absence of the [BOS] token.

C.2. Mistral Analysis

Mistral exhibits slightly different characteristics, which can be attributed to its two-phase training strategy. Initially trained with full attention on sequences matching the sliding window size, the model retains a position-zero attention sink. However, as it transitions to sliding window attention, its reliance on this early sink mechanism diminishes.

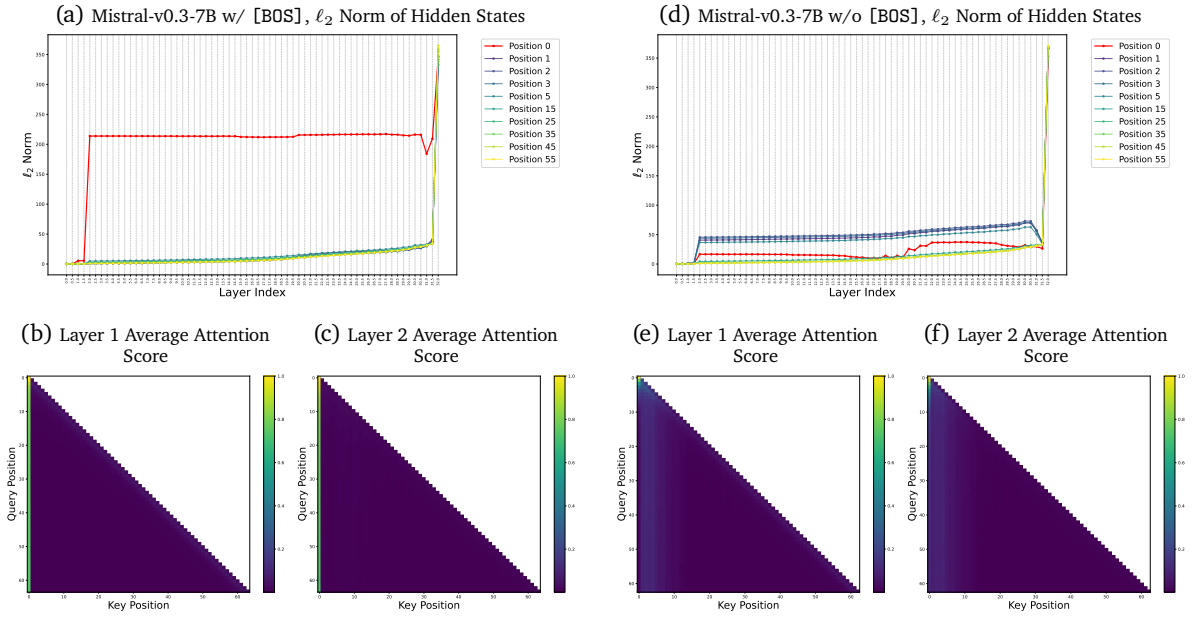


Figure 12: Layer-wise ℓ_2 norm of hidden states and attention score heat maps in . Half-integer indices correspond to the output of attention modules after residual connection. Removing the [BOS] token eliminates the layer-1 attention sink and its associated ℓ_2 norm amplification. However, due to renewed norm growth before layer 2, a position-zero (P0) sink re-emerges in the attention maps even in the absence of the [BOS] token.

C.3. Pythia Series Analysis

Smaller Pythia models such as Pythia-14M and Pythia-70M do not exhibit the emergence of a position-zero sink circuit. Notably, Pythia-160M fails to produce reliable statistics under float16 due to numerical instability. Interestingly, because all Pythia models are trained from scratch on the same number of tokens, we observe a non-monotonic trend as model size increases: larger models, despite having greater capacity, also face increased optimization difficulty, leading to a U-shaped pattern where the emergence layer of the sink first decreases and then increases. This suggests a trade-off between model expressivity and training convergence under fixed compute and data budgets.

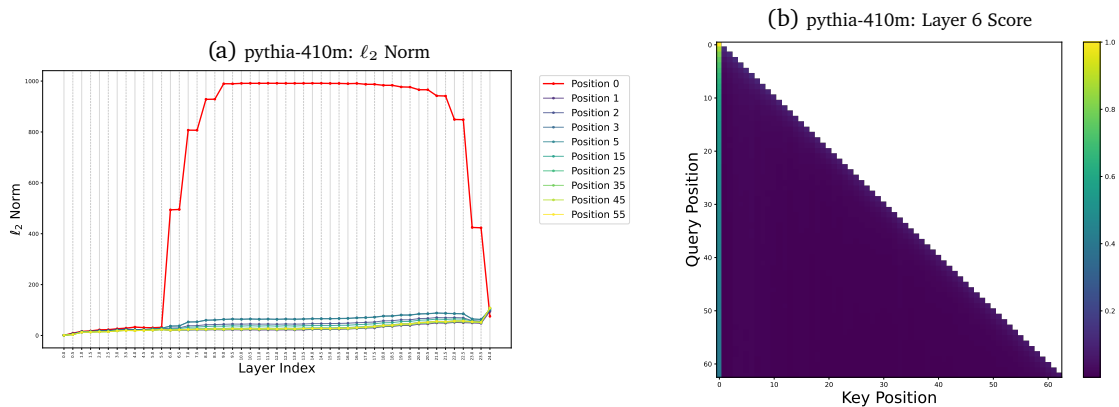


Figure 13: Layer-wise ℓ_2 norm and attention sink visualization for pythia-410m. The attention sink becomes prominent after layer 6, coinciding with the sharp increase in the ℓ_2 norm at position zero (P0).

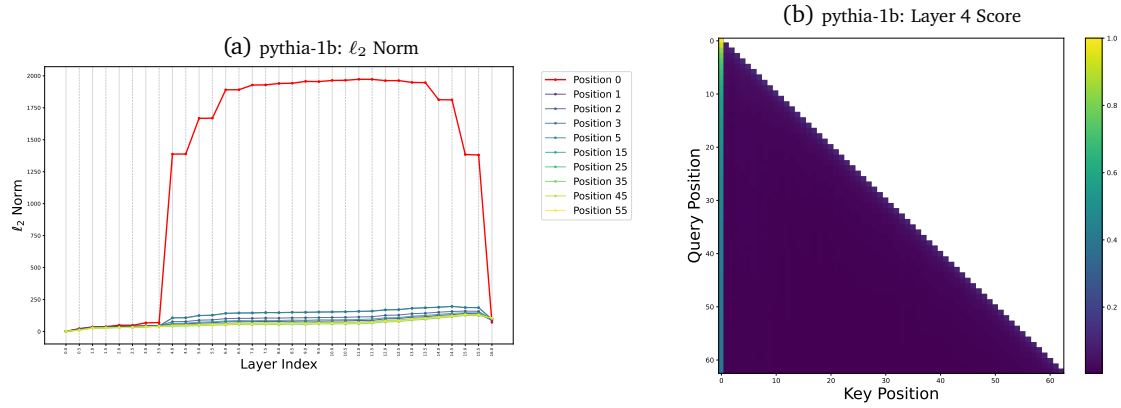


Figure 14: Layer-wise ℓ_2 norm and attention sink visualization for pythia-1b. The attention sink becomes prominent after layer 4, coinciding with the sharp increase in the ℓ_2 norm at position zero (P0).

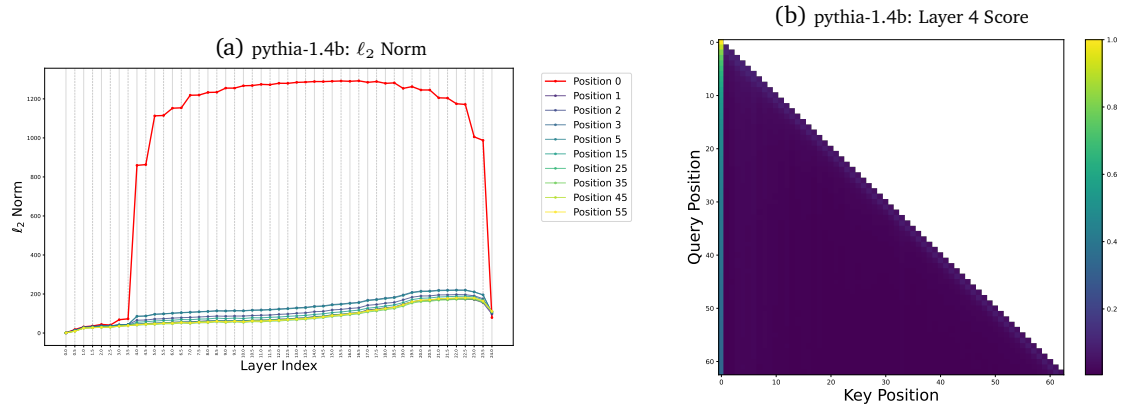


Figure 15: Layer-wise ℓ_2 norm and attention sink visualization for pythia-1.4b. The attention sink becomes prominent after layer 4, coinciding with the sharp increase in the ℓ_2 norm at position zero (P0).

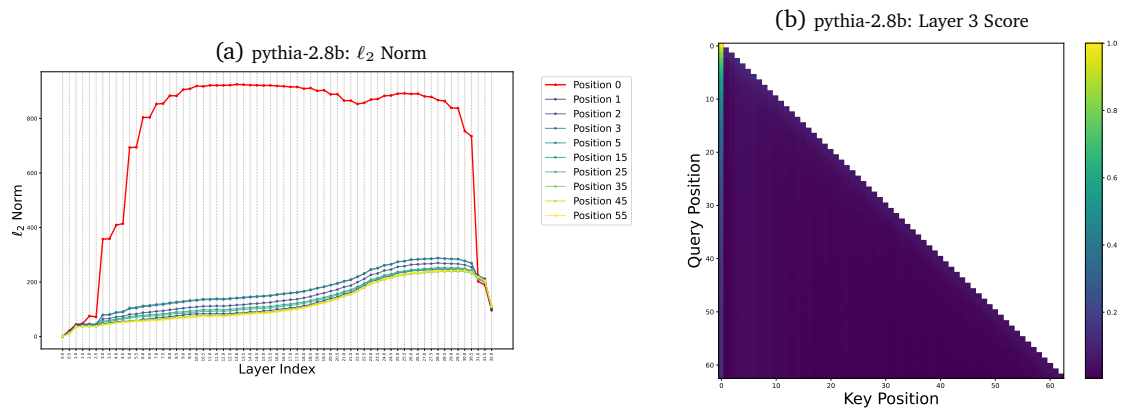


Figure 16: Layer-wise ℓ_2 norm and attention sink visualization for pythia-2.8b. The attention sink becomes prominent after layer 3, coinciding with the sharp increase in the ℓ_2 norm at position zero (P0).

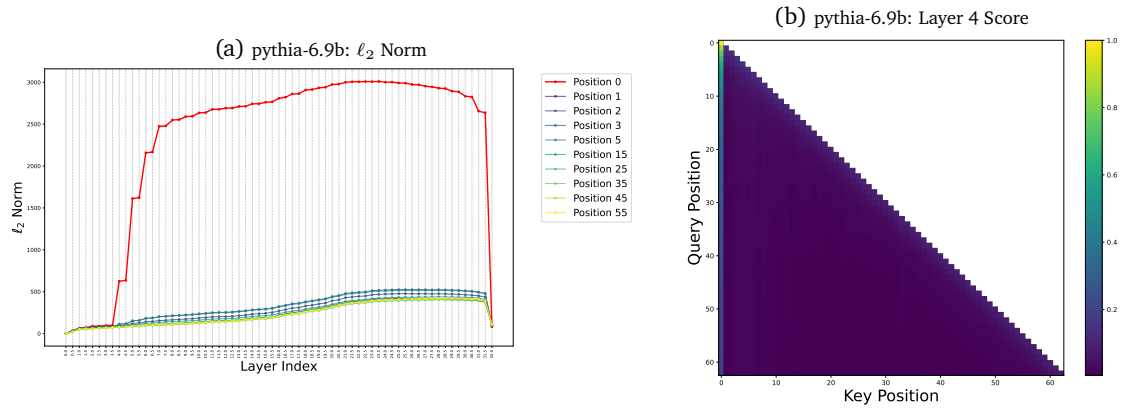


Figure 17: Layer-wise ℓ_2 norm and attention sink visualization for pythia-6.9b. The attention sink becomes prominent after layer 4, coinciding with the sharp increase in the ℓ_2 norm at position zero (P0).

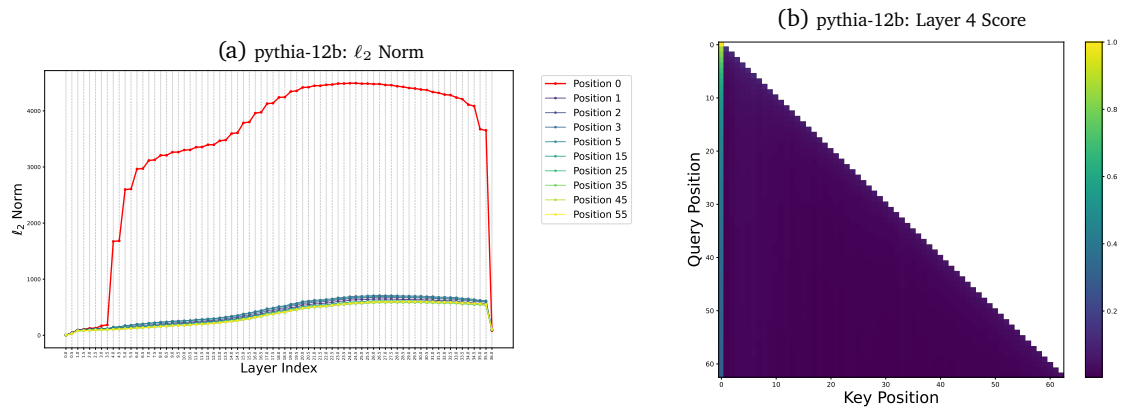


Figure 18: Layer-wise ℓ_2 norm and attention sink visualization for pythia-12b. The attention sink becomes prominent after layer 4, coinciding with the sharp increase in the ℓ_2 norm at position zero (P0).

C.4. Qwen2.5 Series Analysis

By analyzing the Qwen2.5 series, we observe that models of different sizes are allocated varying training budgets. As a result, the final layer in which the sink-related circuit emerges shows no consistent pattern across model scales. Nevertheless, it is important to note that Qwen2.5 models were likely trained independently from scratch rather than derived from a single backbone. This helps explain why the 72B model achieves the best performance: it is not only the largest in size but also appears to be in the final stage of training and has likely received the most extensive token exposure.

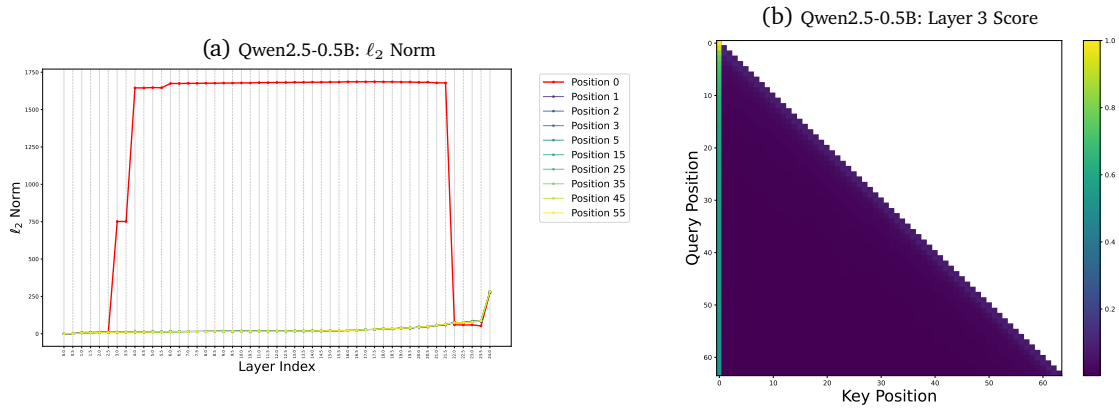


Figure 19: Layer-wise ℓ_2 norm and attention sink visualization for Qwen2.5-0.5B. The attention sink becomes prominent after layer 3, coinciding with the sharp increase in the ℓ_2 norm at position zero (P0).

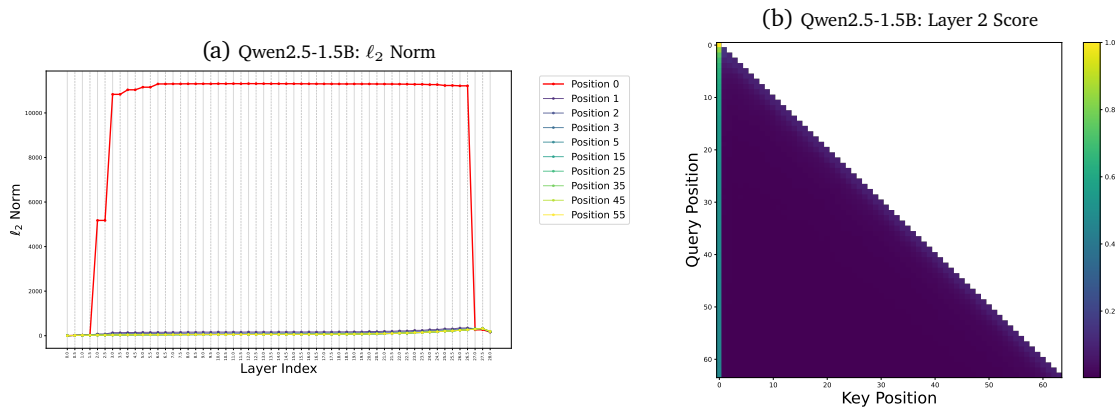


Figure 20: Layer-wise ℓ_2 norm and attention sink visualization for Qwen2.5-1.5B. The attention sink becomes prominent after layer 2, coinciding with the sharp increase in the ℓ_2 norm at position zero (P0).

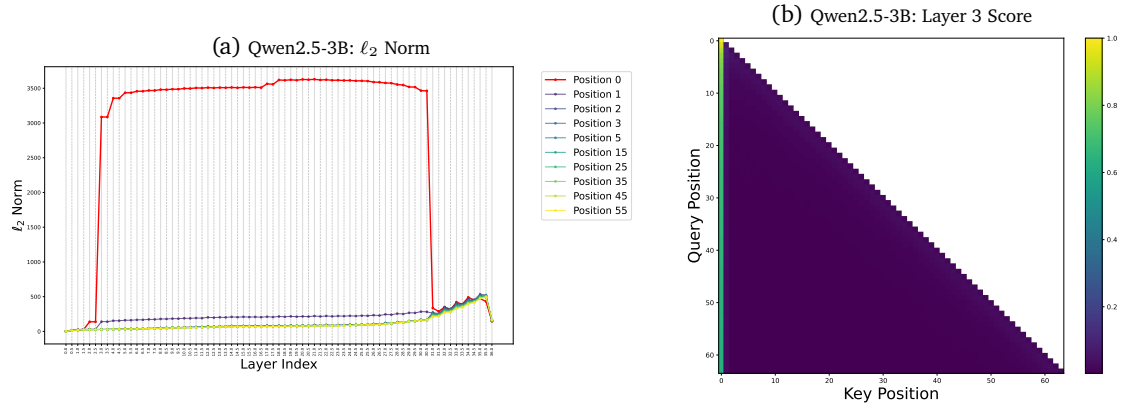


Figure 21: Layer-wise ℓ_2 norm and attention sink visualization for Qwen2.5-3B. The attention sink becomes prominent after layer 3, coinciding with the sharp increase in the ℓ_2 norm at position zero (P0).

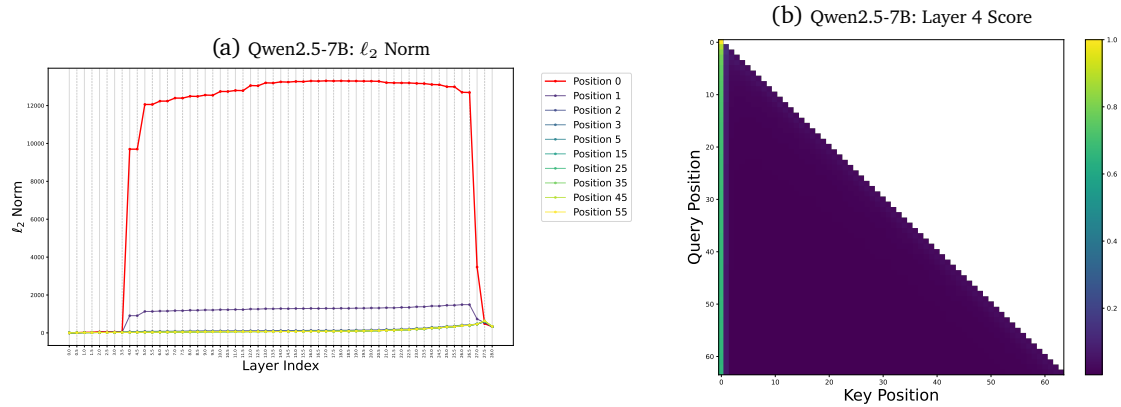


Figure 22: Layer-wise ℓ_2 norm and attention sink visualization for Qwen2.5-7B. The attention sink becomes prominent after layer 4, coinciding with the sharp increase in the ℓ_2 norm at position zero (P0).

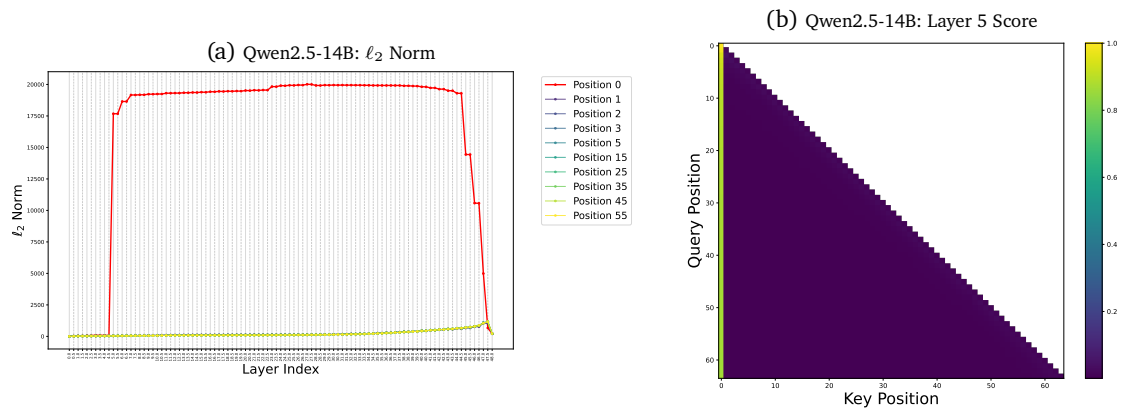


Figure 23: Layer-wise ℓ_2 norm and attention sink visualization for Qwen2.5-14B. The attention sink becomes prominent after layer 5, coinciding with the sharp increase in the ℓ_2 norm at position zero (P0).

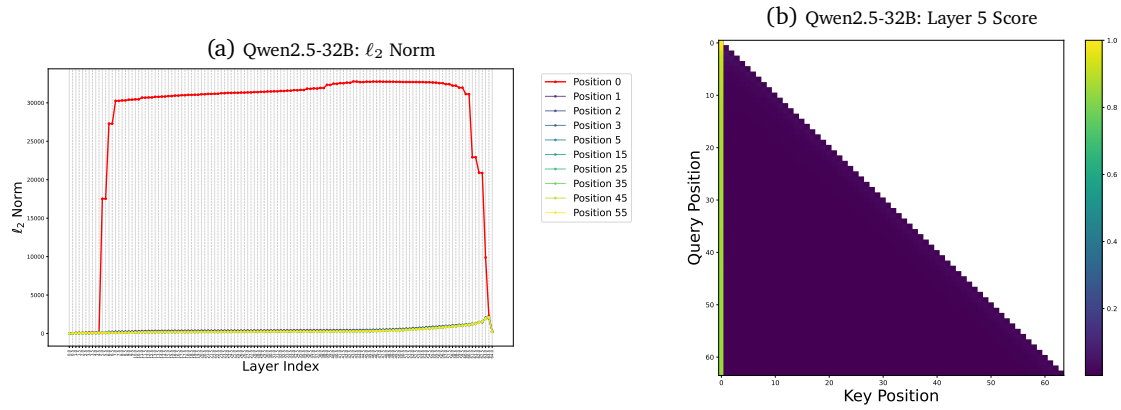


Figure 24: Layer-wise ℓ_2 norm and attention sink visualization for Qwen2.5-32B. The attention sink becomes prominent after layer 5, coinciding with the sharp increase in the ℓ_2 norm at position zero (P0).

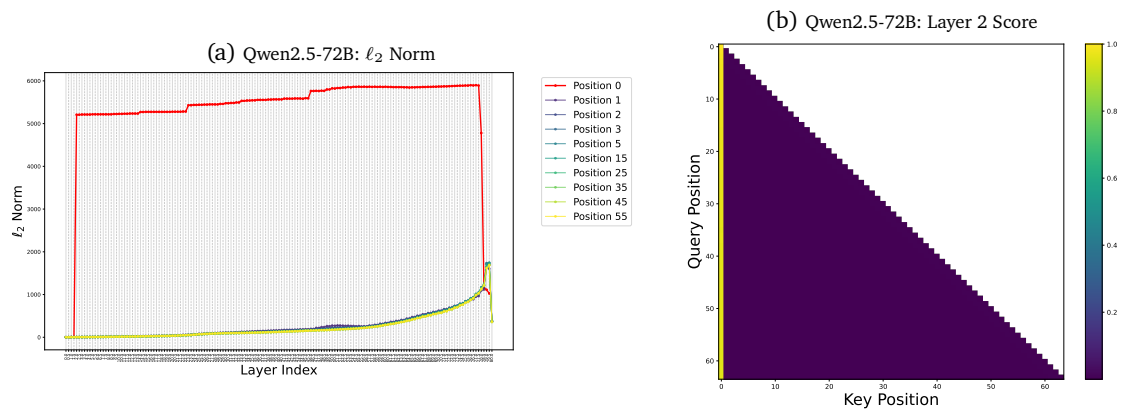


Figure 25: Layer-wise ℓ_2 norm and attention sink visualization for Qwen2.5-72B. The attention sink becomes prominent after layer 2, coinciding with the sharp increase in the ℓ_2 norm at position zero (P0).

C.5. Qwen3 Series Analysis

Our analysis of the Qwen series leads to several key observations. First, the Qwen3 models with 0.6B and 1.7B parameters exhibit highly similar behaviors, notably compressing the sink-related circuit into the first three layers. Second, although the 4B, 8B, 14B, and 32B variants of Qwen3 differ in depth, they all exhibit a strikingly consistent pattern: the attention sink becomes prominent at layer 7, coinciding with a sharp increase in the ℓ_2 norm at position zero (P0). This consistency suggests that these models may not have been trained independently from scratch. Instead, it is likely that one of them served as a base model, with the others produced through scaling or pruning.

Moreover, in contrast to Qwen2, this behavior in Qwen3 suggests that it was trained on a smaller yet higher-quality dataset. Such data efficiency may explain why Qwen3 is able to achieve strong performance even before the sink circuit is fully compressed into the earliest layers. This observation provides additional insight into the design and training strategy of the Qwen3 family, pointing toward improved data curation and possible architectural reuse.

Additionally, we observe that supervised fine-tuning (SFT) does not alter this pattern.

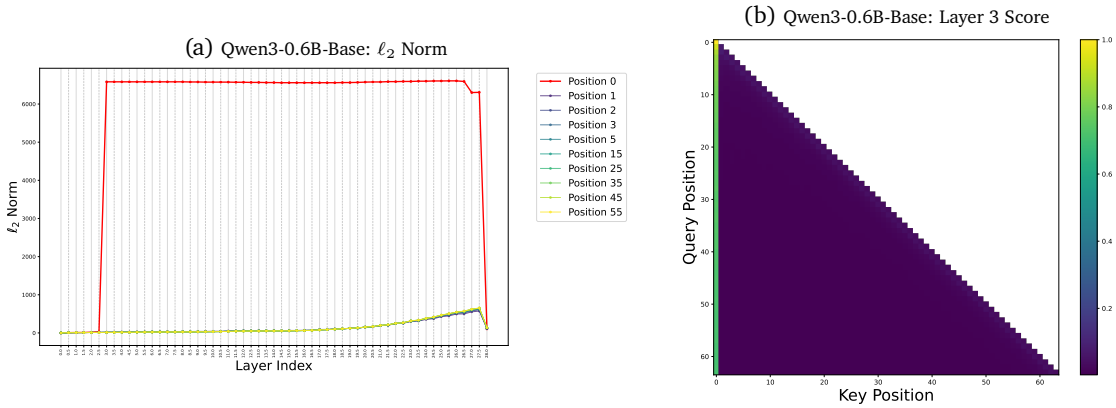


Figure 26: Layer-wise ℓ_2 norm and attention sink visualization for Qwen3-0.6B-Base. The attention sink becomes prominent after layer 3, coinciding with the sharp increase in the ℓ_2 norm at position zero (P0).

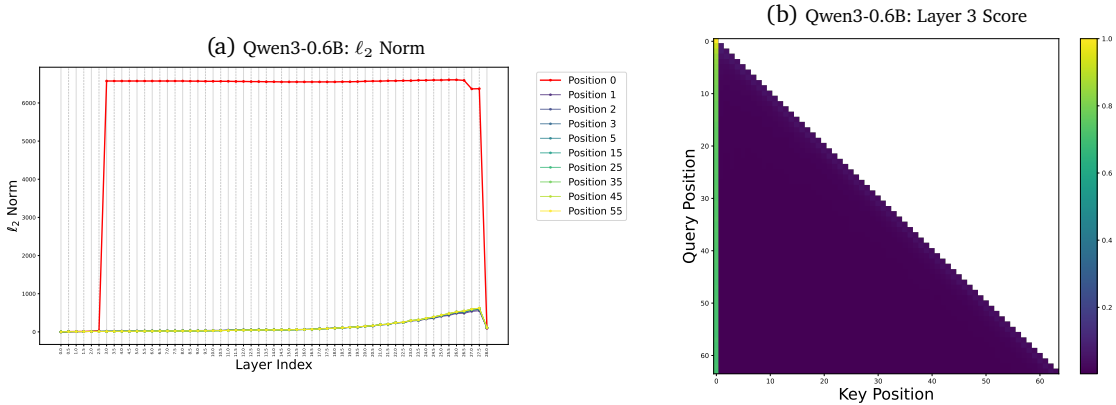


Figure 27: Layer-wise ℓ_2 norm and attention sink visualization for Qwen3-0.6B. The attention sink becomes prominent after layer 3, coinciding with the sharp increase in the ℓ_2 norm at position zero (P0).

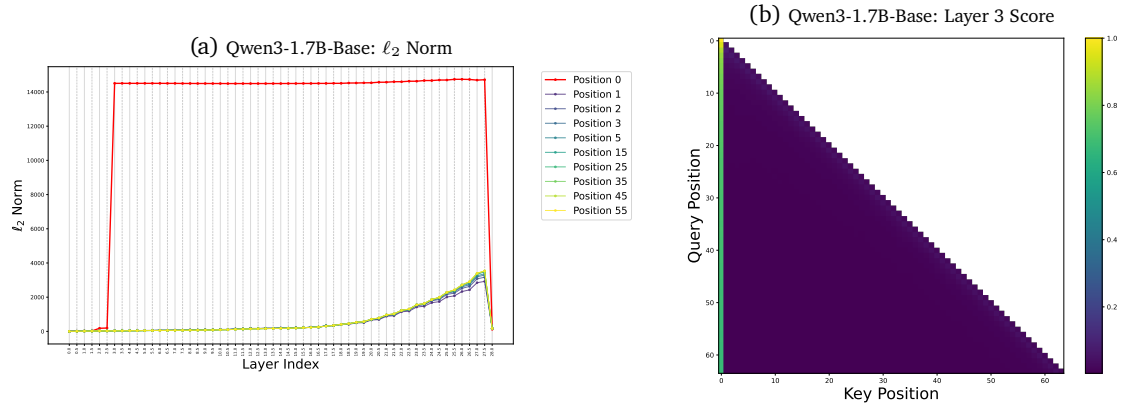


Figure 28: Layer-wise ℓ_2 norm and attention sink visualization for Qwen3-1.7B-Base. The attention sink becomes prominent after layer 3, coinciding with the sharp increase in the ℓ_2 norm at position zero (P0).

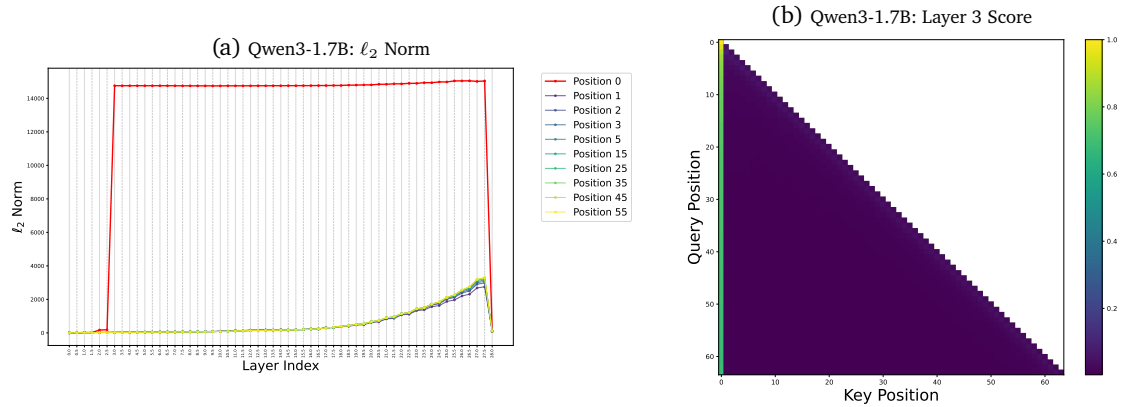


Figure 29: Layer-wise ℓ_2 norm and attention sink visualization for Qwen3-1.7B. The attention sink becomes prominent after layer 3, coinciding with the sharp increase in the ℓ_2 norm at position zero (P0).

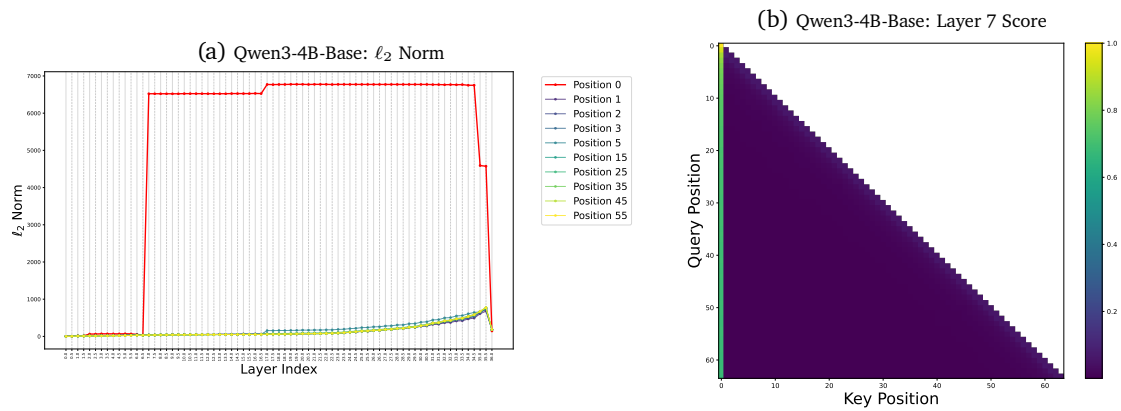


Figure 30: Layer-wise ℓ_2 norm and attention sink visualization for Qwen3-4B-Base. The attention sink becomes prominent after layer 7, coinciding with the sharp increase in the ℓ_2 norm at position zero (P0).

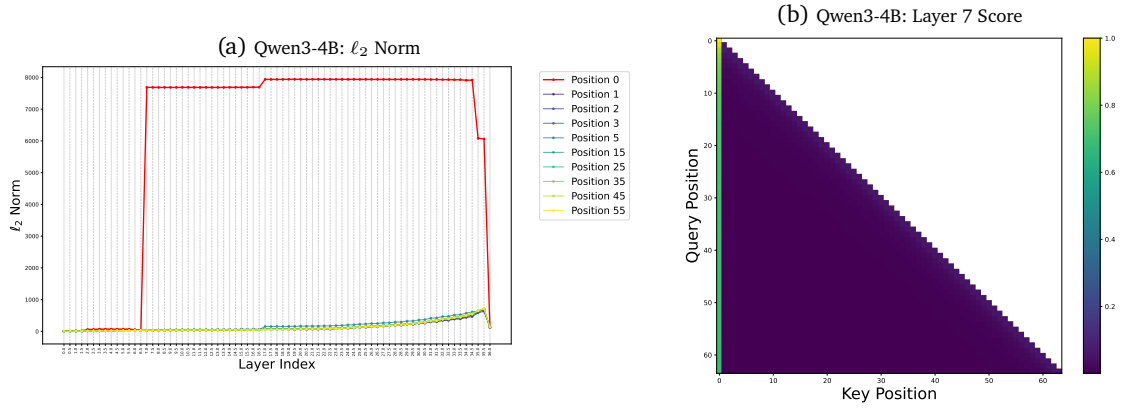


Figure 31: Layer-wise ℓ_2 norm and attention sink visualization for Qwen3-4B. The attention sink becomes prominent after layer 7, coinciding with the sharp increase in the ℓ_2 norm at position zero (P0).

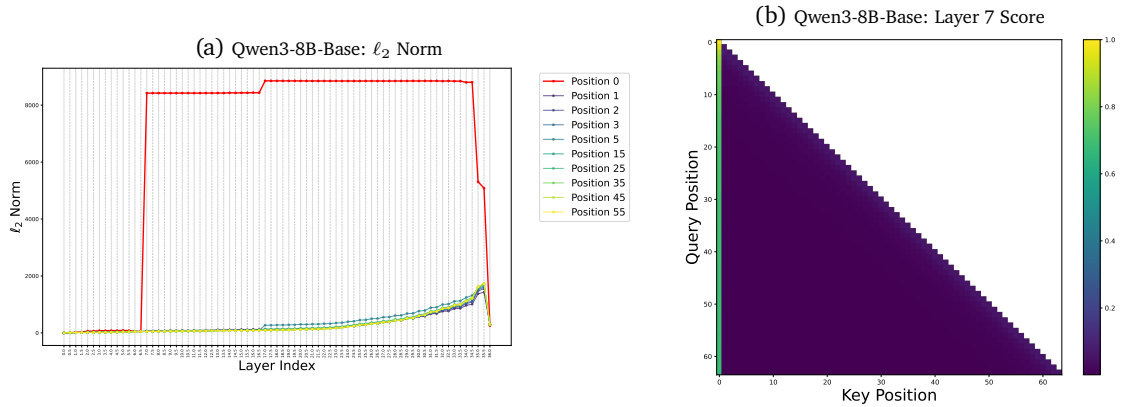


Figure 32: Layer-wise ℓ_2 norm and attention sink visualization for Qwen3-8B-Base. The attention sink becomes prominent after layer 7, coinciding with the sharp increase in the ℓ_2 norm at position zero (P0).

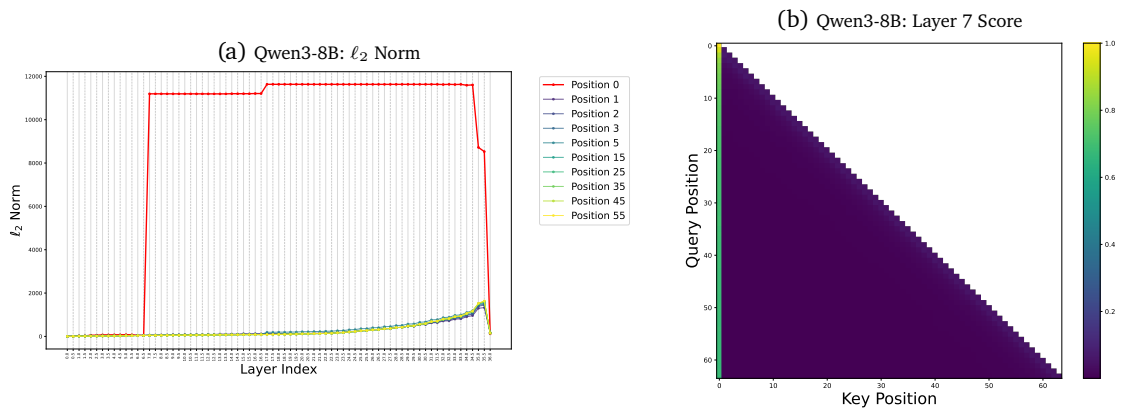


Figure 33: Layer-wise ℓ_2 norm and attention sink visualization for Qwen3-8B. The attention sink becomes prominent after layer 7, coinciding with the sharp increase in the ℓ_2 norm at position zero (P0).

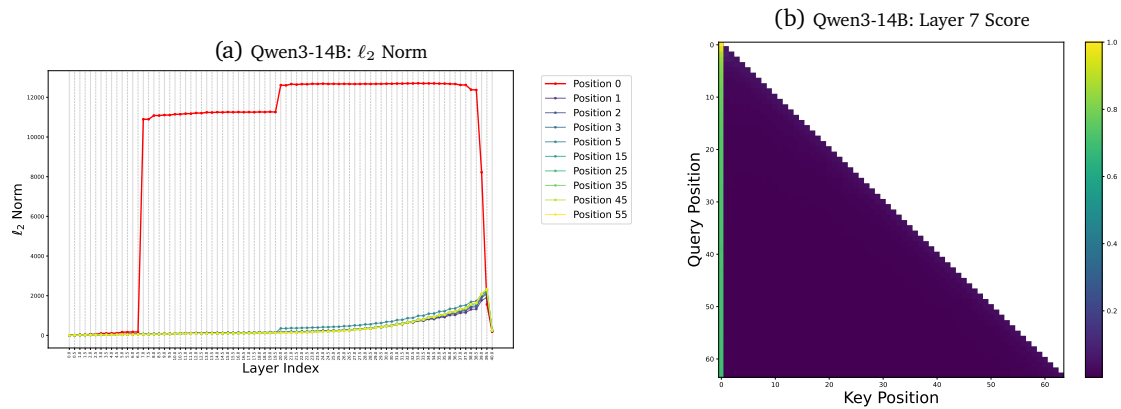


Figure 34: Layer-wise ℓ_2 norm and attention sink visualization for Qwen3-14B. The attention sink becomes prominent after layer 7, coinciding with the sharp increase in the ℓ_2 norm at position zero (P0).

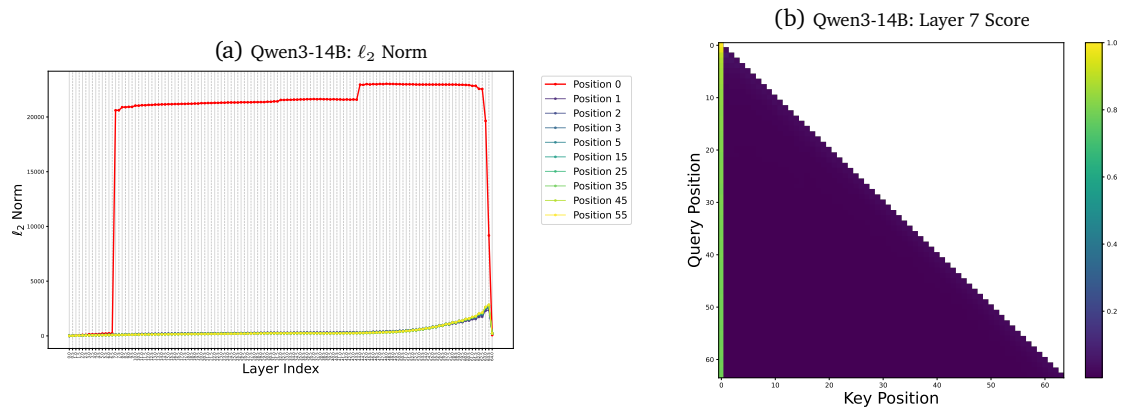


Figure 35: Layer-wise ℓ_2 norm and attention sink visualization for Qwen3-14B. The attention sink becomes prominent after layer 7, coinciding with the sharp increase in the ℓ_2 norm at position zero (P0).

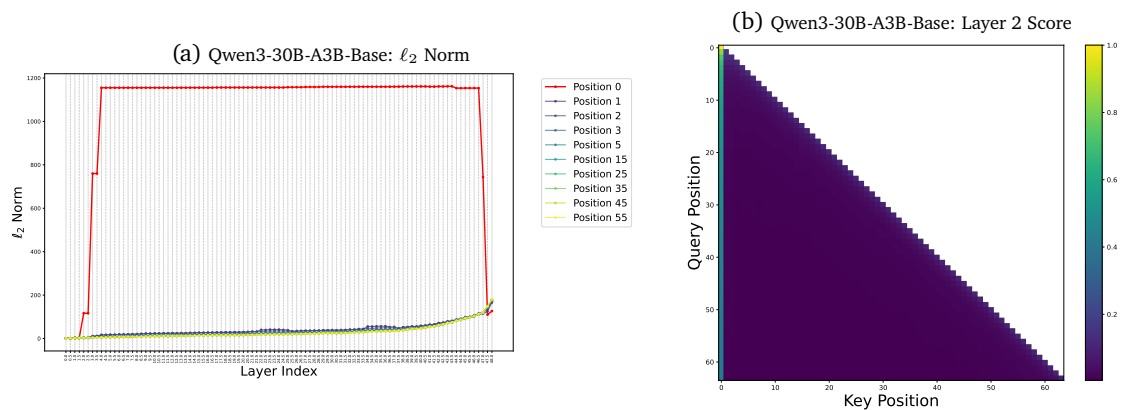


Figure 36: Layer-wise ℓ_2 norm and attention sink visualization for Qwen3-30B-A3B-Base. The attention sink becomes prominent after layer 2, coinciding with the sharp increase in the ℓ_2 norm at position zero (P0).

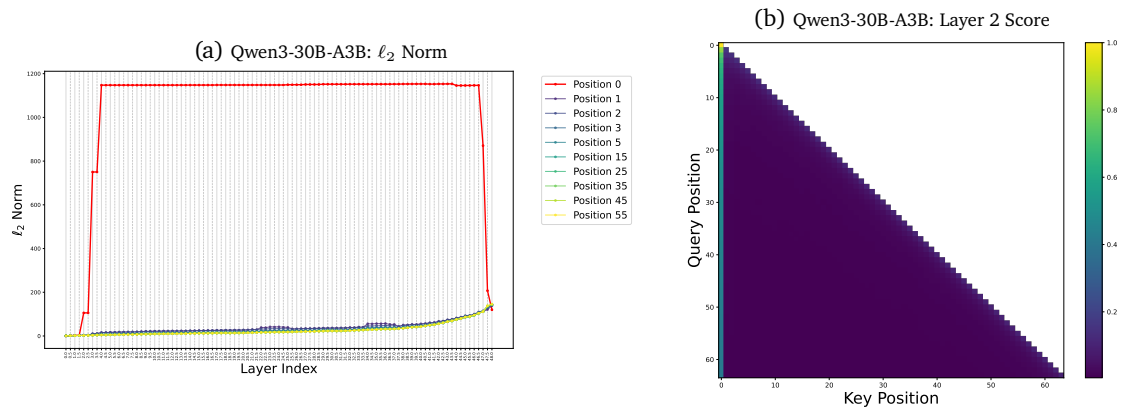


Figure 37: Layer-wise ℓ_2 norm and attention sink visualization for Qwen3-30B-A3B. The attention sink becomes prominent after layer 2, coinciding with the sharp increase in the ℓ_2 norm at position zero (P0).

C.6. Olmo3 Series Analysis

Olmo-3 adopts a hybrid architecture that combines full attention with a sliding window mechanism. Unlike Mistral, which requires a warm-up phase using full attention over shorter sequences to bootstrap learning, this hybrid design appears capable of training with sliding-window attention from scratch. A notable consequence is that, while Mistral still retains a persistent P0 sink, Olmo-3 exhibits no such pattern natively. Due to the lack of controlled comparisons between Olmo-3 and equivalent full-attention architectures, the downstream impact of this architectural choice remains unclear. We therefore report this observation without drawing further conclusions.

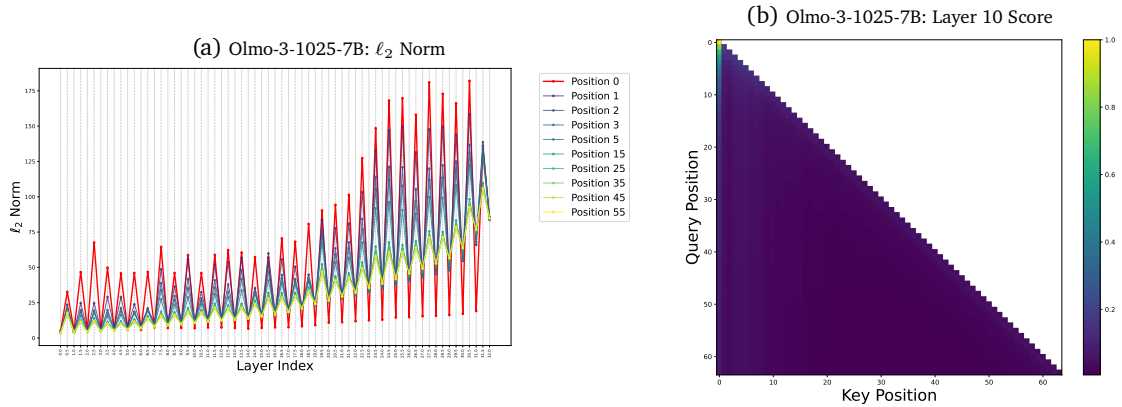


Figure 38: Layer-wise ℓ_2 norm and attention sink visualization for Olmo-3-1025-7B. The attention sink becomes prominent after layer 10, coinciding with the sharp increase in the ℓ_2 norm at position zero (P0).

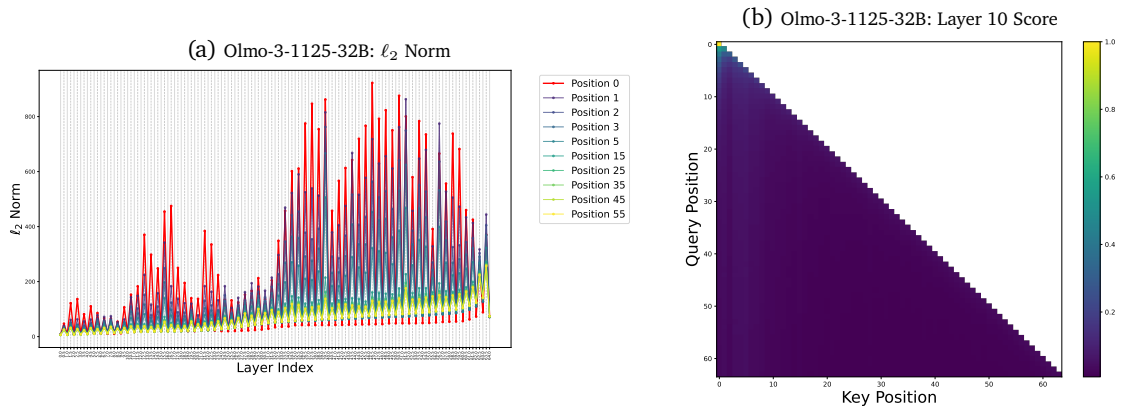


Figure 39: Layer-wise ℓ_2 norm and attention sink visualization for Olmo-3-1125-32B. The attention sink becomes prominent after layer 10, coinciding with the sharp increase in the ℓ_2 norm at position zero (P0).

C.7. OPT Series Analysis

Unlike many modern pretrained language models, the OPT series continues to adopt the original additive absolute positional encoding scheme—a method largely phased out due to its lack of extrapolation capability. This architectural choice allows the position embedding to directly influence the hidden states. As a result, the emergence of the P0 sink in OPT does not depend on an internal identification circuit, as observed in other models, but instead behaves more like models with explicit [BOS] tokens, where the sink effect is tightly coupled with the absolute position of the first token. Because removing the additive positional encoding would trigger severe out-of-distribution behavior, we do not conduct ablation experiments on OPT. Nonetheless, we include these models here for completeness.

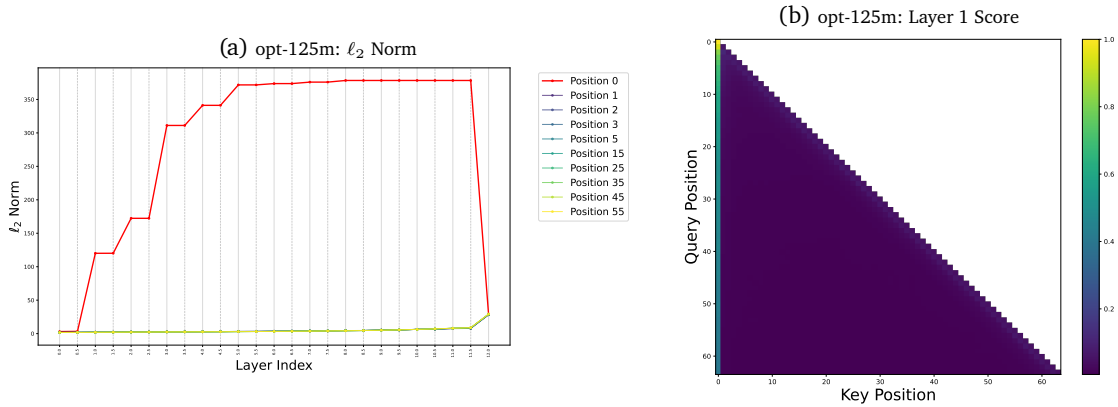


Figure 40: Layer-wise ℓ_2 norm and attention sink visualization for opt-125m. The attention sink becomes prominent after layer 1, coinciding with the sharp increase in the ℓ_2 norm at position zero (P0).

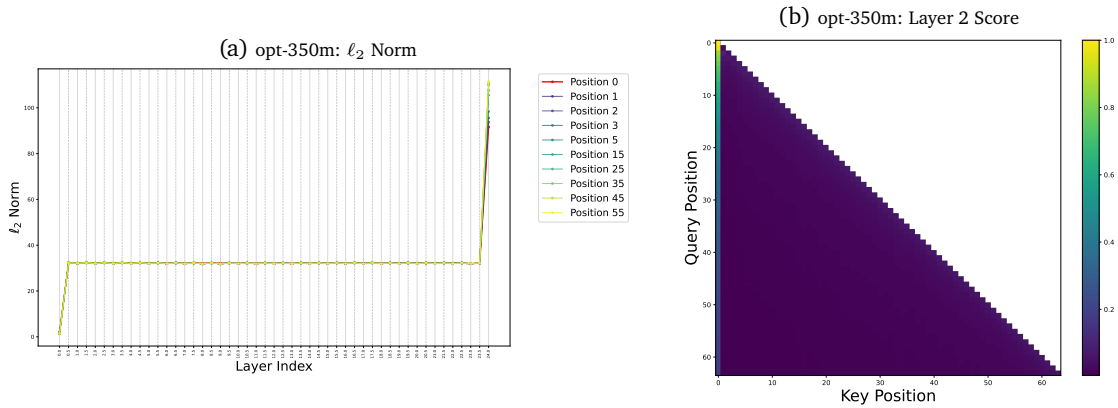


Figure 41: Layer-wise ℓ_2 norm and attention sink visualization for opt-350m. The attention sink becomes prominent after layer 2, coinciding with the sharp increase in the ℓ_2 norm at position zero (P0).

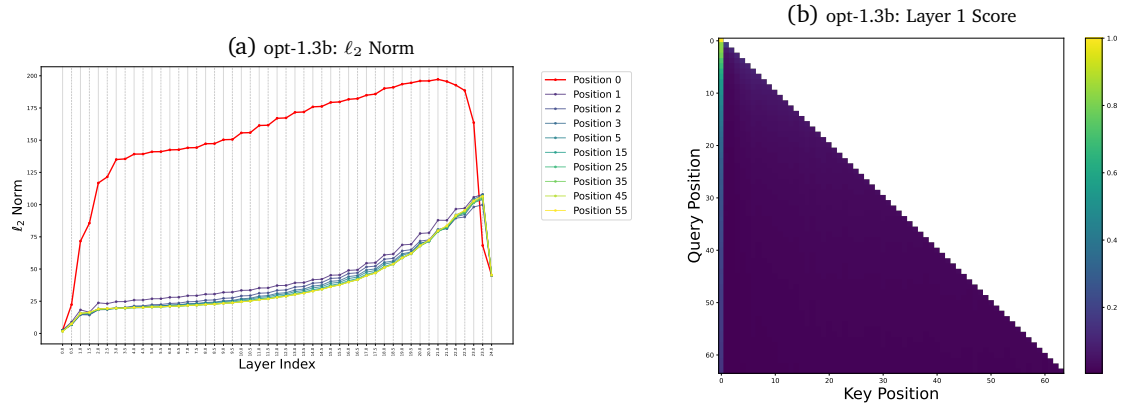


Figure 42: Layer-wise ℓ_2 norm and attention sink visualization for opt-1.3b. The attention sink becomes prominent after layer 1, coinciding with the sharp increase in the ℓ_2 norm at position zero (P0).

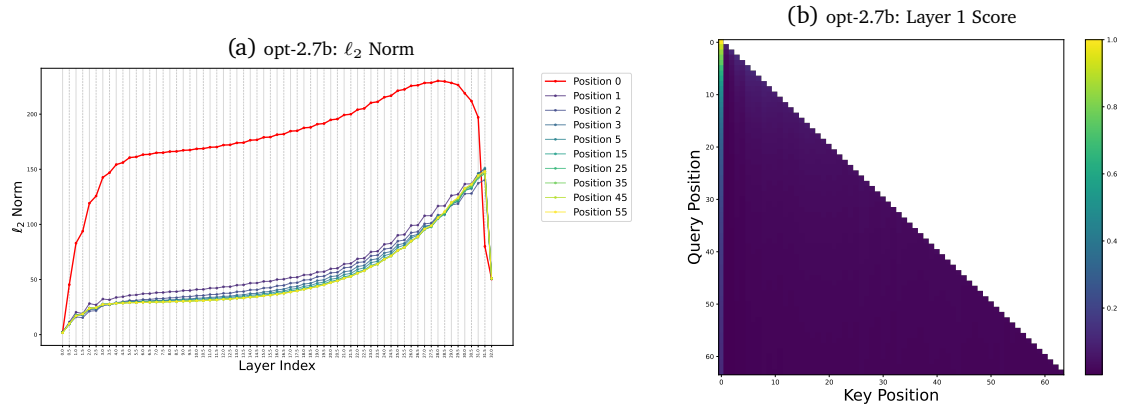


Figure 43: Layer-wise ℓ_2 norm and attention sink visualization for opt-2.7b. The attention sink becomes prominent after layer 1, coinciding with the sharp increase in the ℓ_2 norm at position zero (P0).

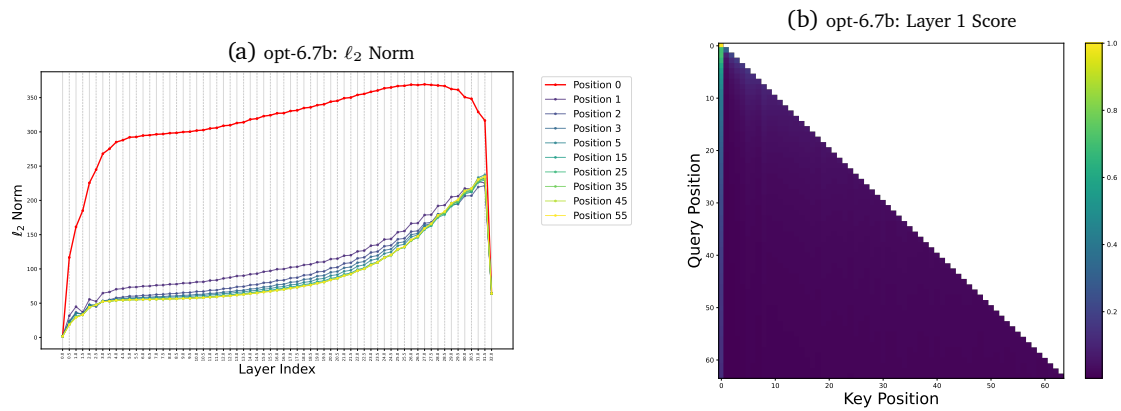


Figure 44: Layer-wise ℓ_2 norm and attention sink visualization for opt-6.7b. The attention sink becomes prominent after layer 1, coinciding with the sharp increase in the ℓ_2 norm at position zero (P0).

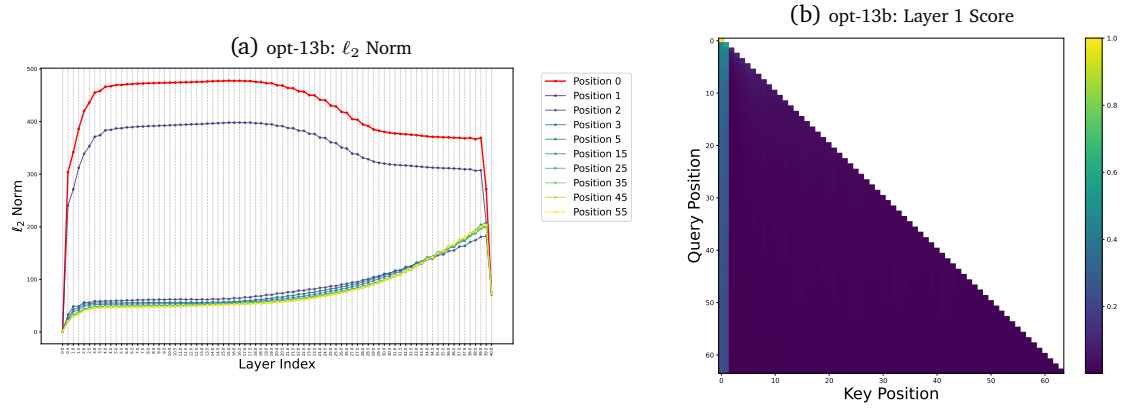


Figure 45: Layer-wise l_2 norm and attention sink visualization for opt-13b. The attention sink becomes prominent after layer 1, coinciding with the sharp increase in the l_2 norm at position zero (P0).

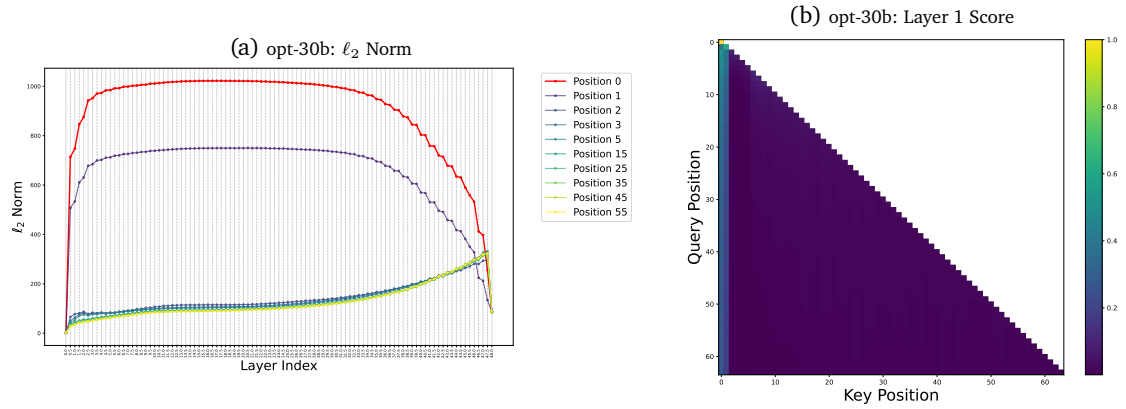


Figure 46: Layer-wise l_2 norm and attention sink visualization for opt-30b. The attention sink becomes prominent after layer 1, coinciding with the sharp increase in the l_2 norm at position zero (P0).

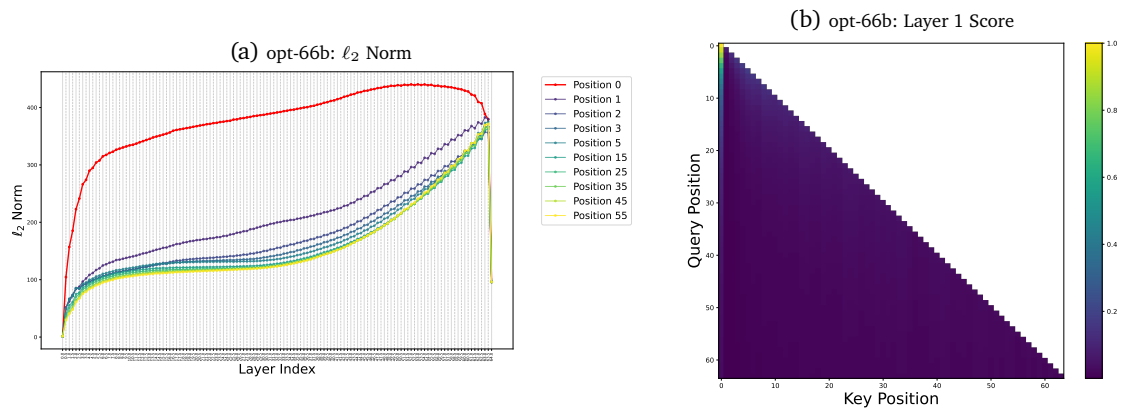


Figure 47: Layer-wise l_2 norm and attention sink visualization for opt-66b. The attention sink becomes prominent after layer 1, coinciding with the sharp increase in the l_2 norm at position zero (P0).